



Updated Reconstruction Methods for Modeling Orion Parachute Loads

Eric S. Ray¹

MRI Technologies (JETS), Houston, TX, 77058

Simulations of the Capsule Parachute Assembly System (CPAS) for Orion descent and landing are anchored to reconstructed flight test data. At the completion of the drop test program, all 25 Engineering Development Unit (EDU) and Qualification flight tests were reconstructed using improved techniques to provide a common set of parameters for Monte Carlo predictions. Multiple data sources are evaluated to augment the reconstruction based on knowledge of inherent measurement errors. Parameters to describe the test data are successively approximated, from initial inspection eventually to comprehensive simulations. Automation was employed to enhance precision and reduce subjectivity. Data from analogous parachutes are combined with appropriate modifications to provide the highest possible statistical significance of the resulting probability distributions. Inflation parameters are examined in multiple dimensions to restrict Monte Carlo dispersions to within physically possible combinations close to observations.

Nomenclature

$(C_D S)(t)$	= Drag area growth as a function of time
$(C_D S)_{i-1}$	= Drag area at the end of previous stage
$(C_D S)_i$	= Drag area at the end of stage i
$(C_D S)_o$	= Full open drag area
$(C_D S)_{peak}$	= Peak drag area during opening or disreefing
$(C_D S)_{p,i}$	= Dynamic drag area of individual parachute i
$(C_D S)_V$	= Effective drag area of payload or test vehicle
CDT	= Cluster Development Test (series)
C_k	= Over-inflation factor
CPAS	= Capsule Parachute Assembly System
DDT	= Drogue Development Test (series)
DGPS	= Differential Global Positioning System
D_o	= Nominal parachute diameter based on reference area, $D_o = \sqrt{4 \cdot S_o / \pi}$
DOF	= Degrees Of Freedom
DSS	= Decelerator System Simulation
EDU	= Engineering Development Unit (test series)
expopen	= Opening profile shape exponent: < 1.0 concave down; = 1.0 linear; > 1.0 concave up
FBCP	= Forward Bay Cover Parachute
F	= Tension force in a parachute riser
g	= Acceleration of Earth Gravity
G	= Load factor (dimensionless)
γ	= Flight path angle
GPS	= Global Positioning System
IMBL	= Instrumented Main Bag Link (for measuring Pilot parachute loads)
IMU	= Inertial Measurement Unit
m_A	= Added mass, $m_A = m_e + m_a$

¹Analysis Engineer, Aerosciences, Flight Dynamics and GN&C, 2224 Bay Area Blvd, Houston, TX, AIAA Senior Member.

m_a	=	Apparent mass
m_e	=	Enclosed mass
MDT	=	Main Development Test (series)
MDTV	=	Medium Drop Test Vehicle (“Medium Dart”)
m_p	=	Mass of parachute and suspension equipment
MPCV	=	Multi-Purpose Crew Vehicle (Orion)
m_v	=	Mass of test vehicle, not including canopies and suspension equipment
n	=	Canopy filling constant, normalized to reference diameter
N_c	=	Number of parachutes in a cluster
n_p	=	Inflation constant (measured in reference diameters) to peak drag area (infinite mass only)
PCDTV	=	Parachute Compartment Drop Test Vehicle
PDT	=	Pilot Development Test (series)
PRF	=	Pressure Recovery Fraction, $PRF = \bar{q} / \bar{q}_\infty = (C_{DS})_p / (C_{DS})_\infty$
PTV	=	Parachute Test Vehicle (Orion “boilerplate” or cone-shaped vehicle for Apollo)
\bar{q}, q_{bar}	=	Dynamic pressure, $\bar{q} = \frac{1}{2} \cdot \rho \cdot V_{air}^2$
\bar{q}_∞	=	Freestream dynamic pressure
ρ, rho	=	Humidity-corrected atmospheric density
RC	=	Ramp Clear (usually chosen as start of test)
RTMU	=	Riser Tension Measuring Units
SAR	=	System Acceptance Review
σ, sigma	=	Standard deviation (general)
S/N	=	Serial Number
S_o	=	Parachute canopy full open reference area based on constructed shape including vents and slots
SPAN	=	Synchronized Position Attitude & Navigation
t_f	=	Canopy fill time from either bag strip or disreef to completion of stage inflation
t_{fp}	=	Time from either bag strip or disreef to occurrence of peak drag area
t_i	=	Inflation start time of either bag strip or the disreef event from a previous stage
θ, theta	=	Fly-out angle for parachute i
t_k	=	Time to ramp down after stage over-inflation
V_{air}	=	Total airspeed relative to air mass
V_i	=	Velocity (airspeed) at beginning of each stage at time t_i
W_p	=	Dry weight of parachute
W_T	=	Total weight of test vehicle, deployed parachutes, and suspension equipment
WTT	=	Wind Tunnel Test
W_v	=	Suspended weight of test vehicle, not including canopies and suspension equipment

I. Introduction

QUALIFICATION flight tests of the Capsule Parachute Assembly System (CPAS) have been successfully completed. The landing system for the Orion/Multi-Purpose Crew Vehicle (MPCV) is moving on to System Acceptance Review (SAR) before human use. Due to limitations of the quantity and capabilities of the flight tests,¹ much of the certification is to be based on high-fidelity Monte Carlo simulations² anchored to collected test data.

Simulation parameters were derived from reconstructions of all seventeen Engineering Development Unit (EDU) and eight Qualification flight tests using the latest data reduction techniques and simulation. All these tests used one of the two flagship test vehicles: either the Orion “boilerplate” Parachute Test Vehicle (PTV)³ for generating a representative capsule wake, or the missile-shaped Parachute Compartment Drop Test Vehicle (PCDTV)⁴ for high-speed testing (Figure 1).



Figure 1. Parachute Test Vehicle (PTV) and the Parachute Compartment Drop Test Vehicle (PCDTV).

This paper documents the CPAS airdrop test reconstruction techniques used, including recently developed changes. A significant effort was made over the course of the test program to constantly improve the accuracy of instrumentation, the capability of imagery, and the fidelity of simulations. Error propagation was studied to indicate where to focus resources to derive the most benefit. Although riser tension is the most critical measurement for parachute performance, there are inherent limitations of measurement accuracy. Flight reconstructions can mitigate load uncertainty by matching the flight vehicle trajectory in simulations. CPAS therefore invested in high-quality Global Positioning System (GPS)/Inertial Measurement Unit (IMU) hardware to minimize uncertainty in velocity (and therefore dynamic pressure) and position.^{5,6}

Early CPAS reconstructions using the FORTRAN-based Decelerator System Simulation (DSS)⁷ treated a parachute cluster as a single composite parachute. Individual loads were estimated based on conservative load share assumptions. Reconstructions were performed by manually adjusting input parameters. A method was developed in Ref. 8 to determine individual parachute inflation parameters from the flight data using the “fminsearch” error function in MATLAB. Although DSS would accept individual parachute inputs, only the total cluster load was output.

The Flight Analysis and Simulation Tool (FAST) was independently developed from the ground up with a high-fidelity individual parachute model. CPAS completely transitioned to using FAST for flight reconstructions and parachute performance predictions. FAST is written in C++ using the Trick simulation architecture and parses python scripts for input. This allows for automation to optimize reconstructions with FAST “in-the-loop” to match peak inflation and disreef loads. Although FAST can simulate 6-Degrees Of Freedom (6-DOF), reconstructions are generally performed with prescribed test vehicle attitudes based on test data (essentially 3-DOF) in order to minimize errors in forebody aerodynamic forces and isolate parachute performance.

Reconstruction of individually measured test parachute loads has greatly increased the number of parachute performance parameter samples available, thereby increasing the statistical significance in the definition of parameter dispersions. Probability distributions relevant to the Orion MPCV are defined in the CPAS “Model Memo”⁹, while distributions associated with drop test parachutes are documented in the CPAS “Test Technique Memo”¹⁰. As more data points became available, distributions that showed a central tendency moved from uniform to normal or lognormal¹¹, resulting in Monte Carlo results becoming more concentrated at representative conditions.

II. Equations and Assumptions

Two redundant methods of determining parachute loads and drag areas are used to complement each other. Total cluster parachute loads can be determined from accelerometer readings, usually from the IMU (after accounting for forebody drag). However, this does not yield information about the relative load share between canopies. Individual parachute load measurements from load cells are converted to individual parachute drag area, $(C_D S)_p$. The individual readings can be calibrated by comparing their sum to the IMU-derived drag area.

The vehicle and parachute system is modelled as multiple bodies with masses connected by a spring. Figure 2 shows a free-body diagram of the forces involved in unsteady parachute deceleration, including the enclosed mass, m_e , and apparent mass, m_a , collectively referred to as “added mass,” m_A .¹² When a vehicle generates a significant wake, its parachute will experience a dynamic pressure, \bar{q} , that is some fraction of the freestream dynamic pressure, \bar{q}_∞ . This ratio is defined as Pressure Recovery Fraction (PRF) and is also equal to the ratio of drag area in a wake to drag area in freestream. Since the local dynamic pressure cannot be directly measured, the freestream dynamic

pressure measured at the vehicle will be referenced. It is therefore convenient to define the quantity $PRF \cdot (C_D S)_p$, which will only be valid for a specific combination of forebody, type of parachute, and number of parachutes in the cluster.

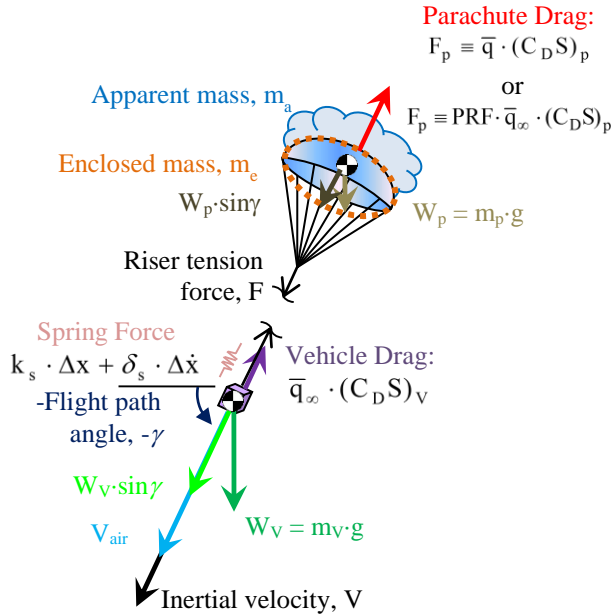


Figure 2. Free-body diagram of a decelerating parachute system.

The terms that comprise the riser tension force, F , are collected in Eq. 1 and will all have to be accounted for in the parachute simulation. While the riser tension force can be directly measured, the total force on the inflating parachute cannot, and is therefore estimated from other measured quantities. The initial reduction of the test data is conducted “offline” (without a full simulation), so only a subset of quantities is considered for computing parachute load. Eventually, using a simulation “in the loop” allows for characterizing all the components of parachute inflation.

$$F = PRF \cdot (C_D S)_p \cdot \bar{q}_\infty + \frac{d(m_e + m_a)}{dt} \cdot V + (m_e + m_a + m_p) \cdot \frac{d(V)}{dt} - W_p \cdot \sin \gamma - k_s \cdot \Delta x - \delta_s \cdot \Delta \dot{x} \quad (1)$$

The load factor, G , measured by the IMU in terms of g , provides a convenient method of approximating the total parachute drag area on the system according to Eq. 2, which was derived in Ref. 8. The total system weight, W_T , is the sum of the vehicle mass, m_v , and parachute dry mass, m_p , multiplied by gravity.

$$PRF \cdot (C_D S)_p \approx \frac{W_T \cdot G}{\bar{q}_\infty} - (C_D S)_v \quad (2)$$

The forebody drag area, $(C_D S)_v$, must be accurately estimated to prevent the introduction of biases in parachute drag estimates. Predicted PTV freefall dynamic pressure errors observed in early Qualification tests exposed a deficiency in the PTV aerodynamic database. A subsequent database update for over-estimated forebody drag revealed that parachute drag had previously been under-estimated. The most accurate method of estimating PTV forebody drag on a particular test is through aerodynamic Development Flight Instrumentation (aeroDFI)¹³ where pressure ports record surface pressures at key locations. These measurements are combined with CFD solutions to characterize the surface pressure distribution, which is integrated to produce the net aerodynamic forces on the vehicle. AeroDFI was available on 11 of 16 PTV tests.

This derived total parachute drag area is compared against the total of individual parachute drag areas approximated by Eq. 3. For large parachutes such as Drogues and Mains, it is important to consider the acceleration of the dry mass of the parachute itself. The load factor measured at the vehicle is used in the absence of local measurements. The implicit assumption is that the primary deceleration of the parachute is aligned with the system

deceleration and velocity vector. The high-fidelity parachute simulation will ultimately track component accelerations in the final reconstruction.

$$\text{PRF} \cdot (C_D S)_{p,i} \approx \frac{F_i + W_{p,i} \cdot G}{\bar{q}_\infty} \quad (3)$$

For small Forward Bay Cover Parachutes (FBCPs), the parachute dry mass is often neglected to simplify to a traditional definition of drag area in Eq. 4.

$$\text{PRF} \cdot (C_D S)_{p,i} \approx F_i / \bar{q}_\infty \quad (4)$$

The legacy method to simulate drag area growth, $(C_D S)(t)$, is to use an exponential curve between the initial drag area from the previous stage, $(C_D S)_{i-1}$, and final drag area for the current stage, $(C_D S)_i$, as shown in Eq. 5. The exponential term defines the shape (expopen < 1.0 is concave down, expopen = 1.0 is linear, and expopen > 1.0 is concave up).

$$(C_D S)(t) = (C_D S)_{i-1} + ((C_D S)_i - (C_D S)_{i-1}) \cdot \left(\frac{(t - t_i)}{t_f} \right)^{\text{expopen}} \quad (5)$$

The fill time, t_f , is normalized to the number of canopy reference diameters, n , travelled during inflation starting at initial velocity V_i . Figure 3 shows a sample drag area growth approximation. The example is finite mass, because the inflation is slow enough to begin decelerating the system before the end of inflation. CPAS Pilot and Main parachutes are modeled as finite mass.

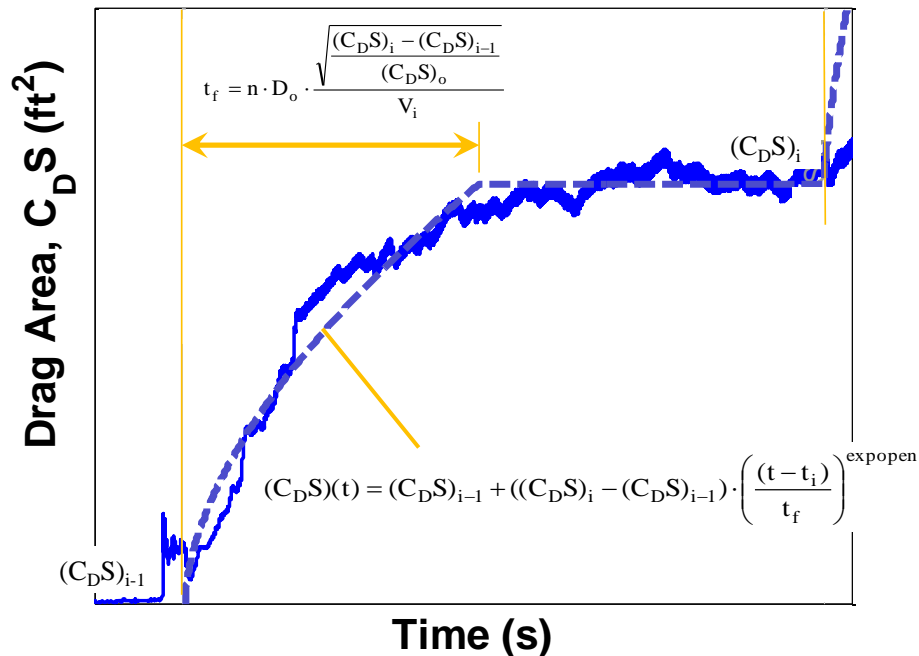


Figure 3. Approximation of finite mass drag area growth.

An infinite mass inflation occurs fast enough that the system does not decelerate during inflation. An example of approaching infinite mass inflation is shown in Figure 4. Infinite mass inflation is usually characterized by an over-inflation, where the drag area growth reaches a peak, $(C_D S)_{\text{peak}}$, before settling down to the steady-state value over time t_k , according to Eq. 6. The over-inflation constant, C_k , describes the magnitude of the peak drag area relative to

the steady-state drag. CPAS FBCPs and Drogues are modeled as infinite mass and C_k is always defined as greater than or equal to 1.0 in CPAS models.

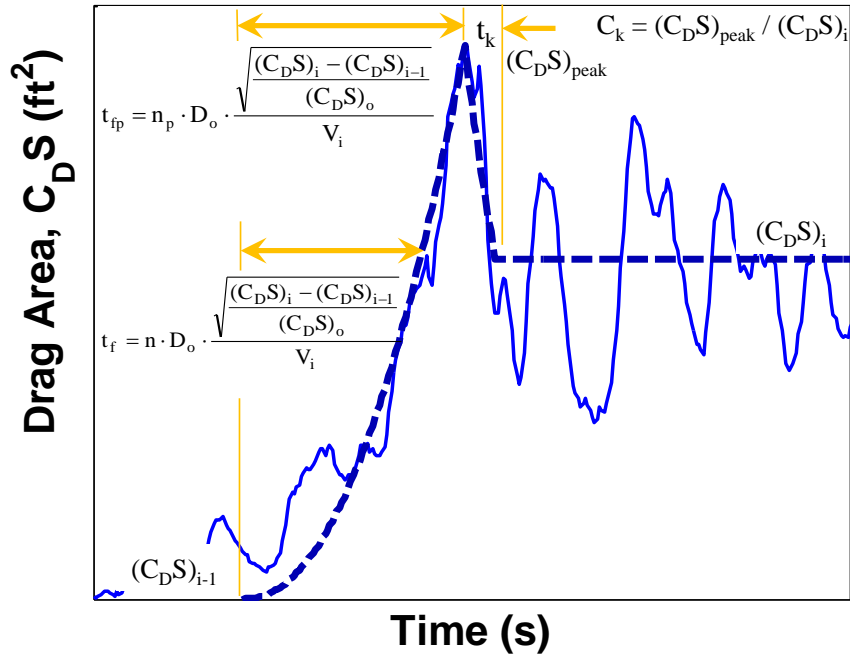


Figure 4. Approximation of infinite mass drag area growth.

$$(C_D S)(t) = (C_D S)_{peak} \cdot (C_k)^{(t_{fp} + t_i - t)/t_k} \quad (6)$$

As discussed in Ref. 14, the drag area growth curve parameters are not independent for infinite mass inflation. In Monte Carlo simulations, varying the C_k and exponent parameters independently can result in unrealistic combinations of those parameters, such as long peak fill times that were never experienced in the flight tests from which the parameters were extracted. Therefore, the fill constant was re-parameterized as explained in Ref. 8 to define the peak fill constant, n_p , which defines the time until peak drag area is reached, t_{fp} . The peak fill constant, exponential term, and over-inflation factor can then be dispersed independently and the results are converted to a standard fill constant for the input file. This ensures that dispersed Monte Carlo cases are within family of the reconstructed test data.

As the risers and suspension lines exit a deploying parachute bag, these elements are re-accelerated to match the velocity of the vehicle, tending to slow it down. FAST models this effect for most parachutes by adding an “inelastic load” which acts through the center of gravity (CG) of the parachute, emulating additional drag imparted on the vehicle. Appropriate values of inelastic load for FBCPs and Drogues are determined empirically. A more physically accurate model was developed for the Main parachutes based on the masses and lengths of the deployment train, and the inelastic load is no longer used for Mains.

The techniques for data reduction and reconstruction are specific for the four CPAS parachutes in Sections III through VI. The factors affecting drag area are summarized in Section VII.

III. Forward Bay Cover Parachute (FBCP) Reconstruction

After Orion jettisons its Forward Bay Cover (FBC), the primary purpose of the 7 ft D_o Conical Ribbon FBCPs is to prevent re-contact, as shown in Cluster Development Test (CDT)-3-14 in Figure 5. This can be accomplished with only two of the three parachutes. Because the FBCPs were not introduced until fairly late in the CPAS development test program, scaled proxy data from Drogues were used to help define performance expectations. Before they were tested using mortar deployment, FBCPs were used as programmers to allow the PCDTV to accelerate to high speed. These tests provided useful data for FBCP steady-state drag area, but static line deployment precluded obtaining relevant inflation parameters.

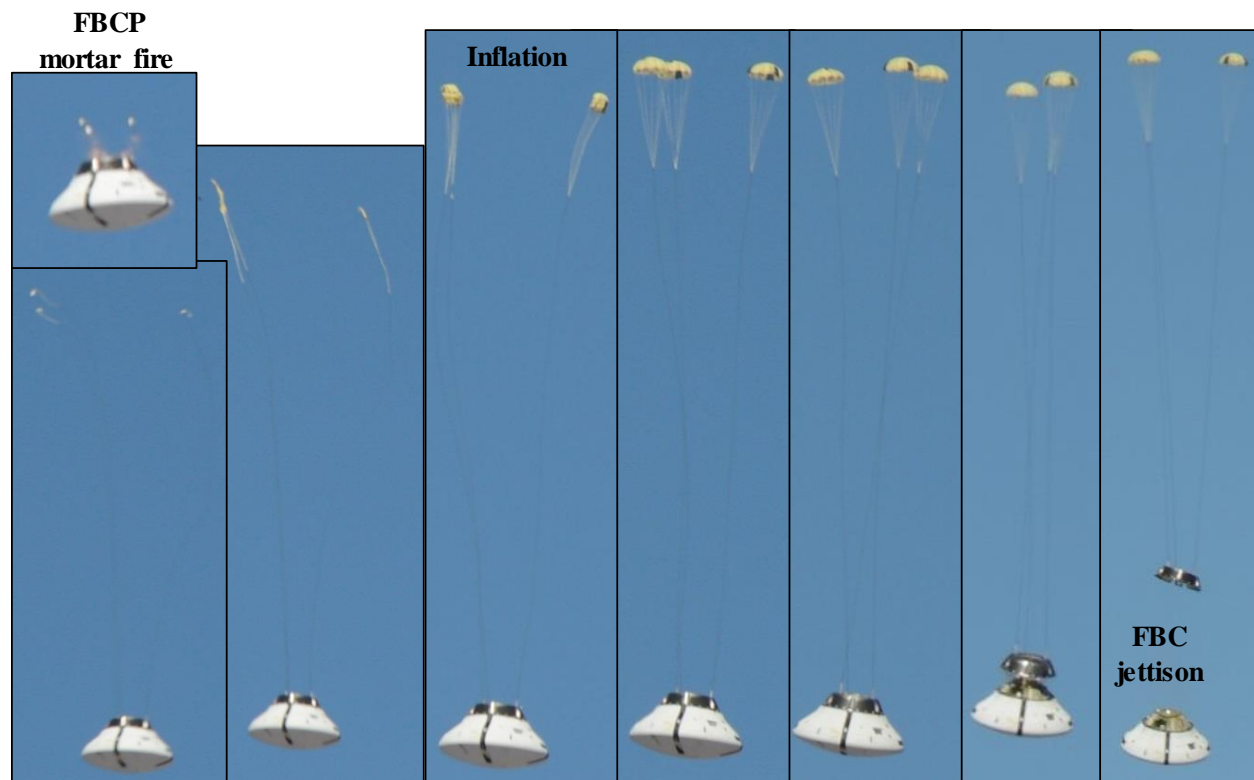


Figure 5. FBCP mortar deployment and FBC jettison from PTV on CDT-3-14.

Because the test program planned relatively few FBC jettison tests, a method was developed to mortar deploy a pair of FBCPs from the tunnel of either a PTV or PCDTV in order to obtain additional FBCP inflation data. Riser Tension Measuring Units (RTMUs) were developed to measure load data, but will not be used on the Orion spacecraft. Independent FBCP load measurements were also available for tunnel-deployed tests from instrumented load pins at single-event fittings below the fairlead. In order to balance data collection with the preference for using of representative Orion hardware on FBC tests, not all FBCP risers were instrumented, and not all instruments successfully recorded usable data. However, the Lockheed Martin Landing Recovery System (LRS) team was able to infer loads data using the FBC flexure data for several FBCPs. This same method was used to estimate FBCP loads on Exploration Flight Test (EFT)-1, as the parachutes were not instrumented. Because FBCP drag is smaller than the drag of the forebody vehicle, IMU-derived drag area is not useful in estimating performance due to relatively high uncertainty.

Cluster Qualification Test (CQT)-4-5 is used as an example of the FBCP reconstruction process. Directly measured RTMU load data were collected from two tunnel-deployed FBCPs. The loads were converted to drag areas using Eq. 4, as plotted in Figure 6. Full open drag area and over-inflation factor were determined by inspection of the drag area history. The MATLAB curve fit algorithm determined the values of peak fill constant, exponential term, and settling time which best fit the data.

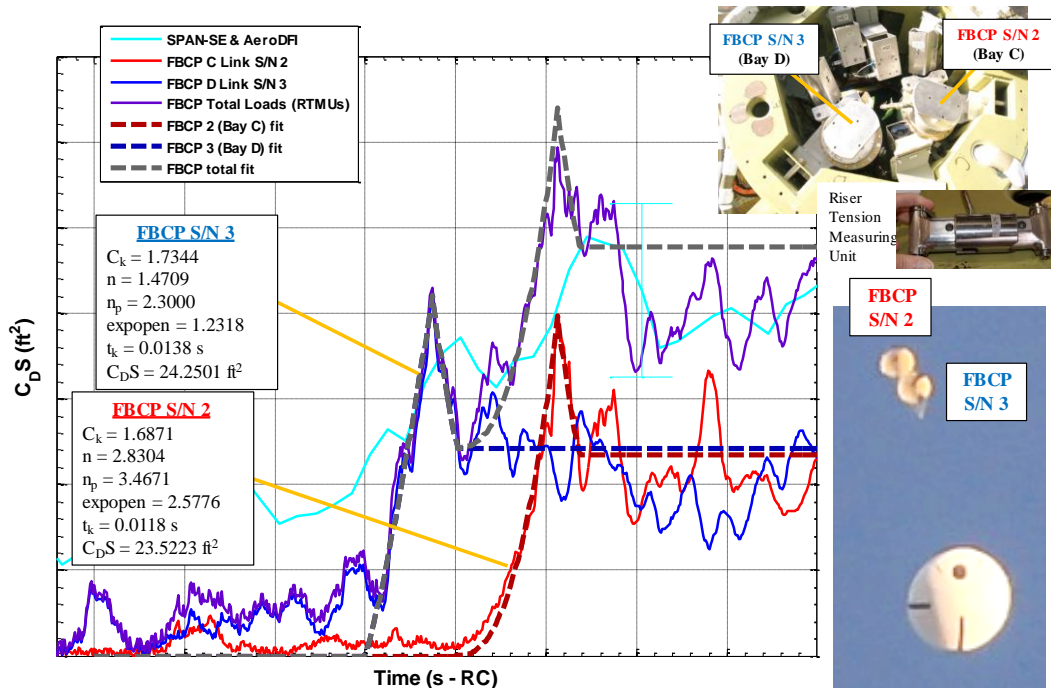


Figure 6. CQT-4-5 FBCP drag area matching (before scaling).

These parameters were used in the FAST input file, which was initialized at FBCP mortar fire using conditions from the flight data. FAST read in the day of flight atmosphere, prescribed PTV attitude, aeroDFI forebody drag data, and vehicle mass properties. Three searches were performed using FAST with simple bifurcation routines written in Python. First, the FBCP mortar velocities were adjusted until each FBCP started inflating at a time consistent with the data. Next, the inelastic load was adjusted until the simulated dynamic pressure of the test vehicle matched the actual value at the time of deployment. The inelastic load was applied uniformly to each FBCP. There was no reason to run these search simulations beyond the deployment times, so a solution could quickly be found. Next the simulation was run through the end of the FBCP phase where the simulated altitude at that time was noted. The resulting peak loads from FAST are higher and later than the measured peak load data, as shown in Figure 7. This should be expected because the test data reduction method neglected the added mass and spring force effects to obtain inflation parameters, but both these effects are modeled in FAST. Matching processed test data that does not include these effects mistakenly attributed their effect to drag area growth, which therefore was slightly exaggerated in FAST.

Several optimization routines were then run sequentially in FAST, resulting in loads traces plotted in Figure 8. First, a constant scale factor was applied uniformly to both average full open drag areas to either increase the parachute drag if the simulated altitude was below the actual measurement, or decrease parachute drag if the simulated altitude was too high. The scale factor was adjusted until the FAST trajectory matched the actual altitude at the end of the stage. Once the trajectory match was satisfactory, the drag scale factor (0.825 in this case) was applied to the original load data to compensate for inherent uncertainties in the riser load measurements. Because RTMU load calibration is only conducted statically, there is uncertainty in dynamic load readings. Next, the mortar velocities and inelastic loads were again searched for until the deployment timing and dynamic pressure match known targets when the simulation used this drag area scale factor.

An additional refinement was conducted to account for the added mass, spring force, and other effects which were neglected when computing drag area. Over-inflation factor and peak fill constant were modified over a number of iterations. The timing and magnitude of the simulated peak inflation load was compared to the scaled riser load test data. If the simulated peak load magnitude did not equal the test data value, then the next candidate C_k was scaled by the ratio of target peak load to the current peak load value. If the simulated time of peak load did not match the data, then the next candidate value of n_p was scaled by the ratio of the desired peak fill time to the current peak fill time value (n_p was converted to n for FAST input). In this way, small changes to the input parameters quickly converged to optimized values such that FAST could exactly match the test peak inflation load magnitude and timing. C_k was reduced significantly and peak fill constant were lowered as well. The optimized parameter values are green and bold in the figure. Notice that the scaled cluster load more closely matches the IMU data. Without this refinement, the statistical distribution of FBCP over-inflation factor would be centered too high, such that Monte Carlo simulations of peak load would be overly conservative.

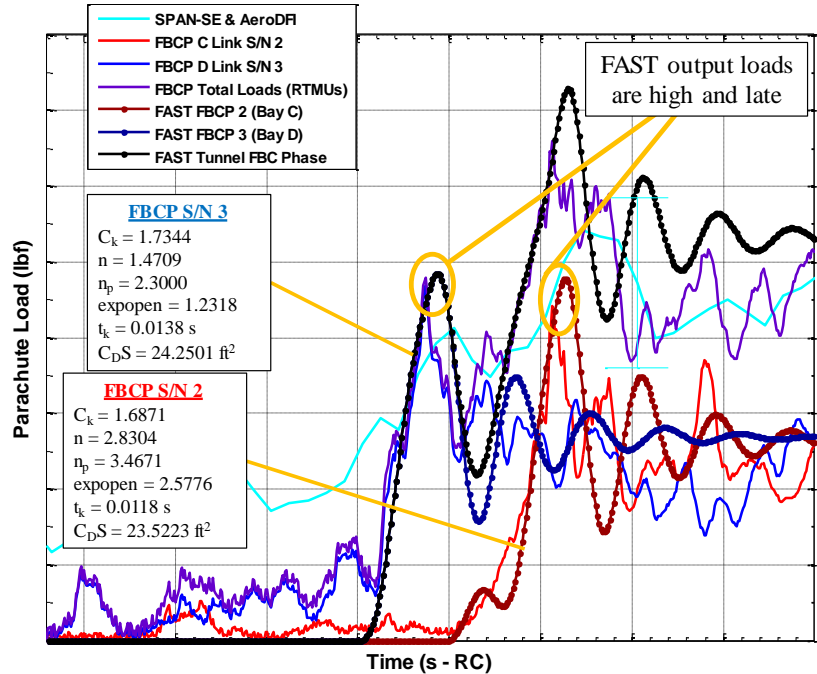


Figure 7. CQT-4-5 FBCP FAST load output (before scaling).

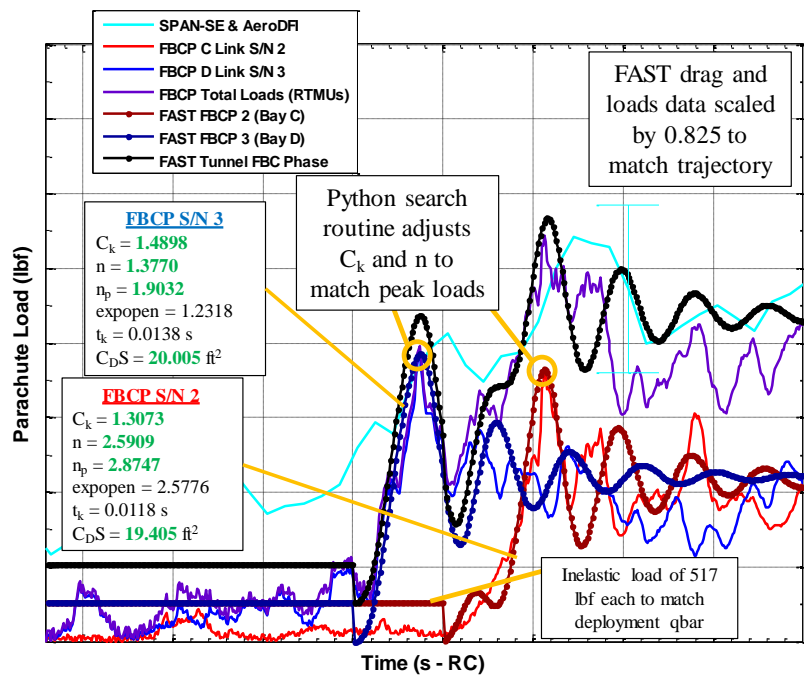


Figure 8. CQT-4-5 FBCP load scaling and peak matching.

IV. Drogue Parachute Reconstruction

The 23 ft D_0 Variable Porosity Conical Ribbon CPAS Drogue parachutes perform the majority of the subsonic deceleration for Orion after reentry. CPAS is designed to function with only one of the two Drogues, if necessary. Most features of the Drogue design were unchanged throughout the CPAS test program, with a notable exception of increased suspension line length ratio for improved full open performance. A wealth of data exists for Drogues because they are often used as programmers, even when not included as test parachutes. To manage peak inflation loads, the CPAS Drogue phase begins with two reefed stages before disreefing to full open. Drogue deployment and staging are shown in Figure 9.

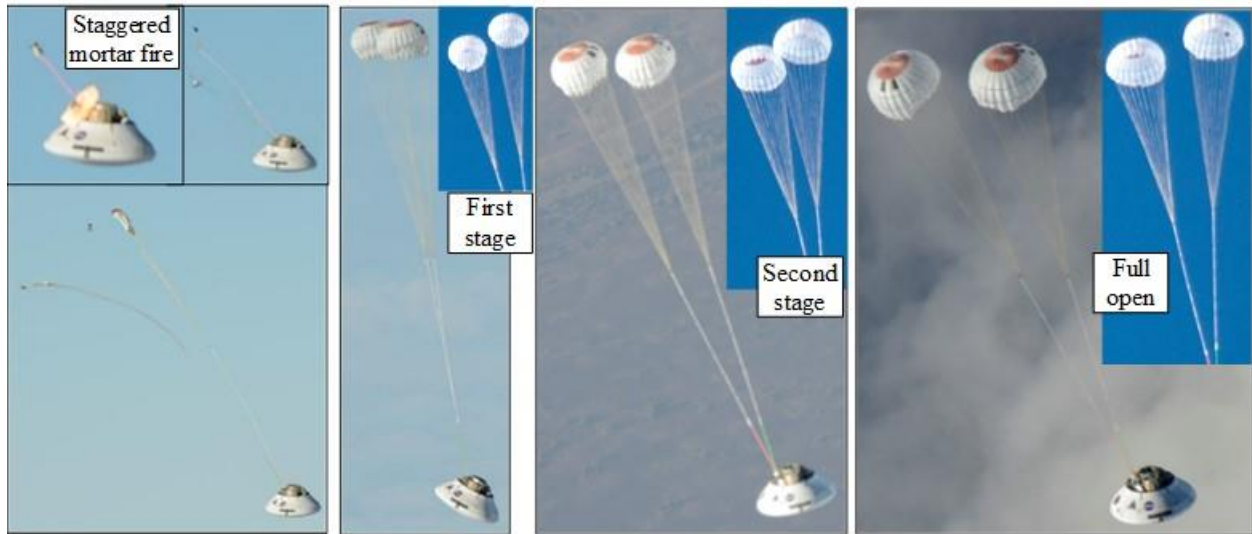


Figure 9. Drogue mortar deployment (left), reefing (center), and full open (right) on CDT-3-15.

Early CPAS tests used in-line strain links for tension measurement. Tests using representative Orion attachment hardware required transitioning to instrumentation below the fairlead of the forward bay “flowerpot” where risers attach to the capsule structure. An earlier design used steel riser extensions to attach to the vehicle. The final design uses Kevlar continuous suspension lines for weight savings and attaches to a concentric pin assembly with attached load bar measurement devices. Both of these latter designs often result in individual riser load readings lower than the IMU load due to “friction losses” as the risers bend over fairleads.

To compensate for this effect, the riser drag areas determined from Eq. 3 are scaled such that the time average of their sum equals the time average of IMU drag area from Eq. 2. The source individual riser load data are scaled using the same factors. The scale factors are specific to each reefing stage, as the friction losses vary with forebody dynamics, which tends to decrease as the parachutes disreef.

A. Drogue First Stage Reconstruction

The Drogue first stage reconstruction process is very similar to that of the FBCPs. CQT-4-5 is again used as an example. Scaled Drogue riser load data were converted to drag area using Eq. 3 (accounting for parachute dry mass), as shown in Figure 10. Stage-specific steady-state drag area and over-inflation factor were determined by inspection. The MATLAB “fminsearch” function was used iteratively to determine the best fit peak fill constant, exponential term, and settling time such that the theoretical drag area growth curve best matched the drag area data.

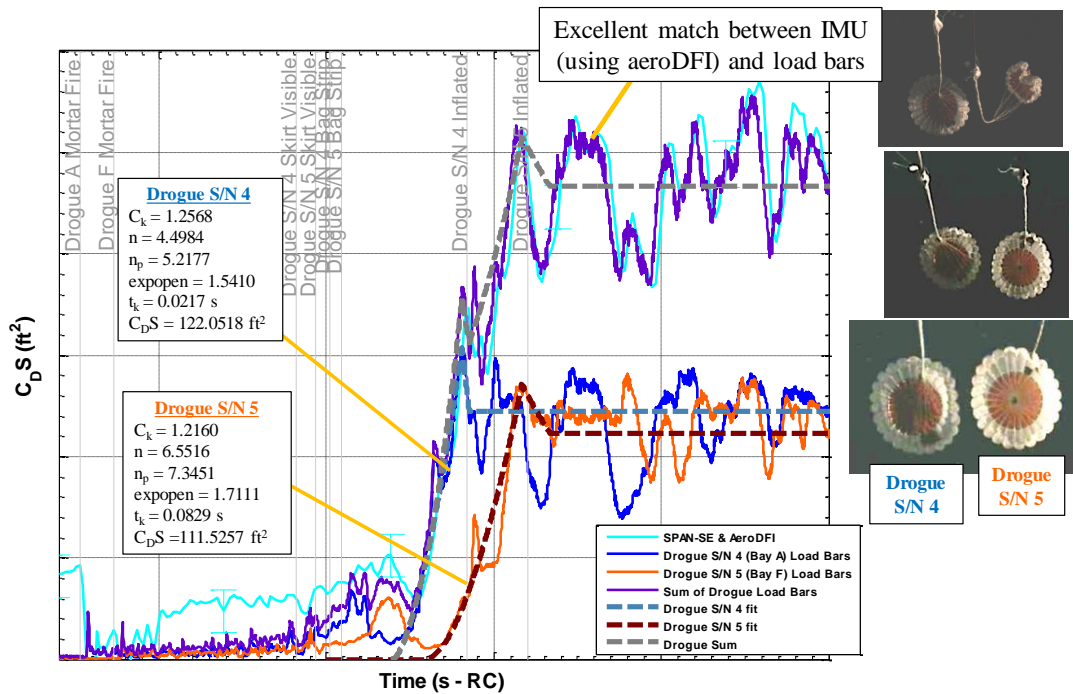


Figure 10. Drogue first stage reconstruction optimization method.

The resulting inflation parameters were transferred to the FAST input file, such that simulated loads could be compared with individual loads data, as plotted in Figure 11. The mortar deployment of CPAS Drogues is staggered by 100 ms. The FAST Drogue simulation was initiated at the first mortar time using state data from the trajectory. The Drogues take independent paths and thus begin inflation at different times. As with the FBCPs, python search

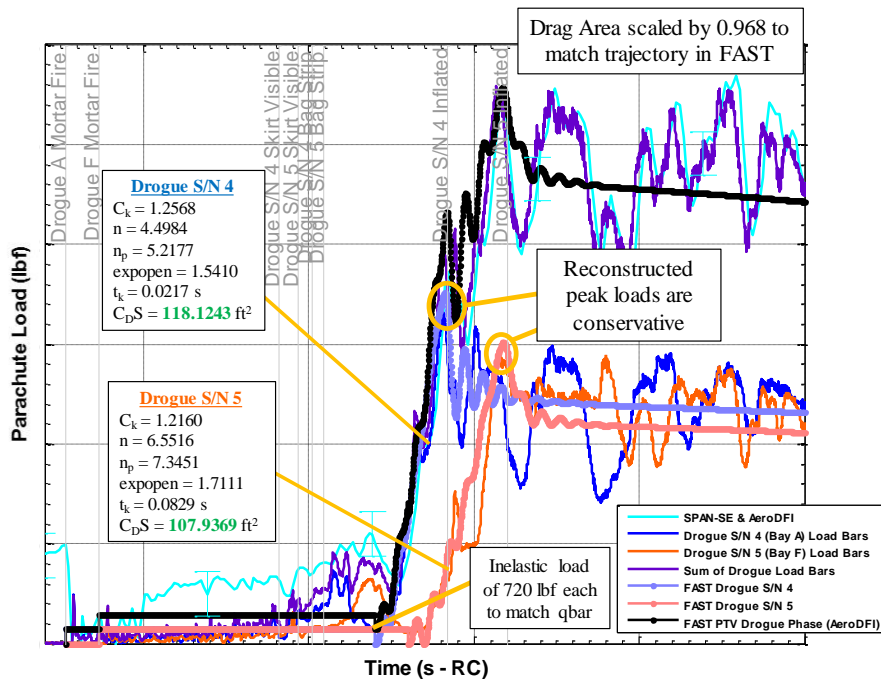


Figure 11. CQT-4-5 Drogue first stage FAST load output.

The updated $C_D S$ values are listed in bold green text. The simulated peak loads are slightly conservative due to the added mass and spring force models present in FAST. The test data show more oscillations than the simulated damped

routines are executed in conjunction with FAST through deployment to obtain the optimum mortar ejection velocities and inelastic load.

A scale factor was applied to the first stage drag of both parachutes in order to match the altitude at the end of first stage using a Python search routine. The search resulted in a scale factor of 0.968. Because such Drogue drag scale factors are very close to unity, the original Drogue load data are not scaled (as is done for the FBCPs). Measurement errors in the Drogue load readings had already been mitigated by applying scale factors to match the IMU-derived drag.

The output individual loads compare favorably to the load data in Figure 11.

response due to many non-modeled effects such as canopy deformations, forebody wake turbulence, and transverse line motion.

Parallel optimizations were then performed with a Python script to adjust FAST input parameters to match the timing and magnitude of the peak loads. The timing was adjusted by increasing or decreasing the peak fill constant (then converting to fill constant) to make the peak occur later or earlier, respectively. Peak load magnitude was established by scaling C_k proportionally to the ratio of the target value to the output value. Because these effects were coupled in the model and because each Drogue acts on the simulated vehicle, adjustments to both parameters were

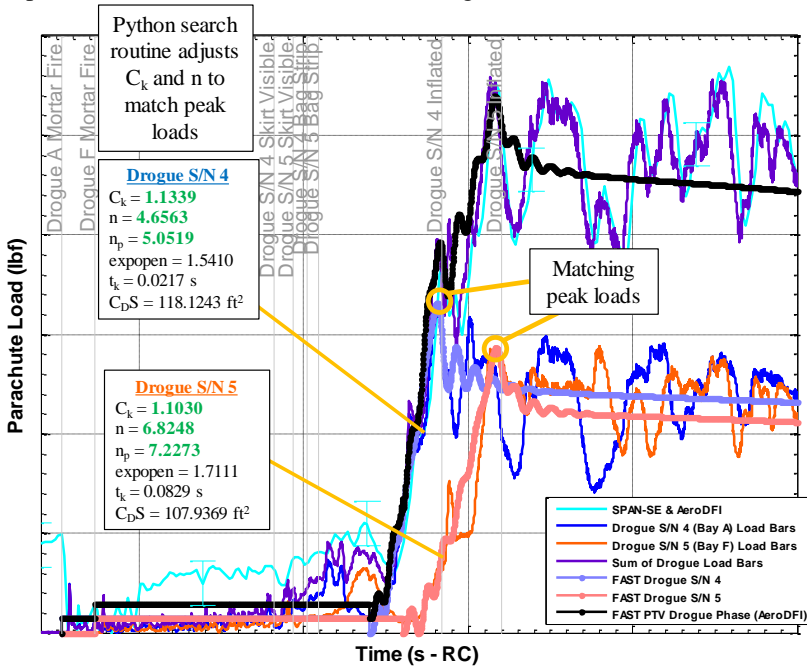


Figure 12. CQT-4-5 Drogue first stage peak load matching.

run simultaneously on both simulated Drogues to incrementally approach the targets with each iteration. The final match of simulation output to the data is shown in Figure 12. The modified inflation parameters that produce the match are noted in bold green text. Note that C_k decreased by about 10% for both Drogues, which was typical.

Despite the automation of this reconstruction technique, one remaining area of subjectivity is the determination of the start time of the inflation growth curve. There is no clear event in the video to denote the start of inflation, though it will always be a finite time after bag strip. The reconstructed parameters are sensitive to the chosen start time.

B. Drogue Disreef Reconstruction

The disreef times for each parachute are usually slightly different, as indicated by sudden drag area growth and confirmed with video observations. MATLAB is used to obtain the best fit inflation parameters to match each disreef event, as show in Figure 13.

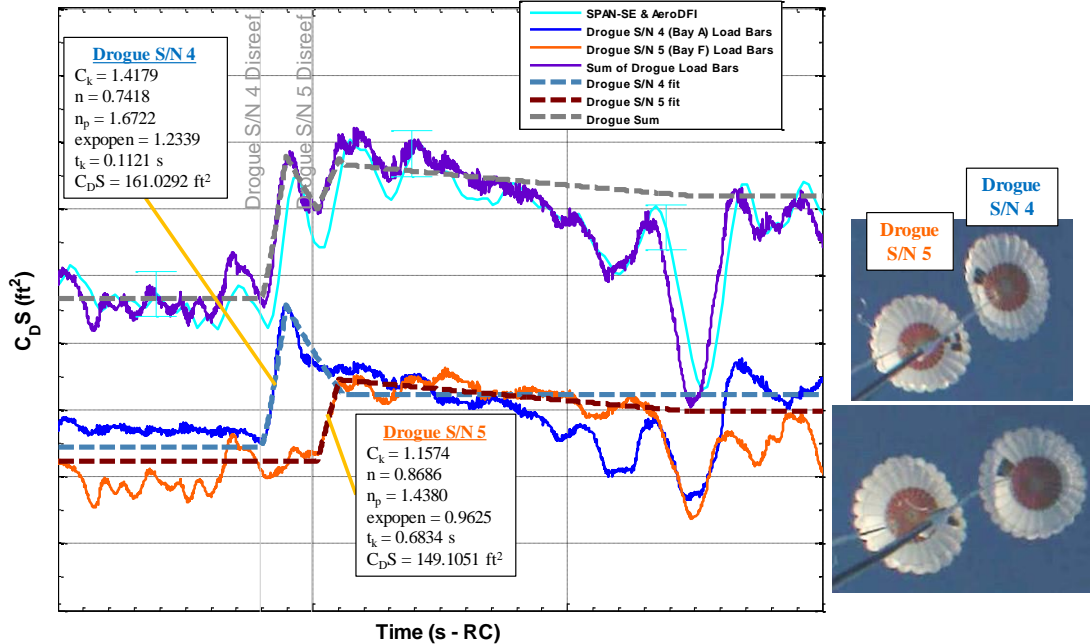


Figure 13. CQT-4-5 Drogue disreef to second stage drag area fit.

Stage duration times are adjusted in the FAST input file such that simulated disreef events match actual timing. Python search routines are then executed in series to obtain the optimum steady-state drag scale factors which will allow FAST to match GPS test altitudes at the end of each reefing stage. The search for the full open scale factor takes the longest because each iteration must simulate the entire Drogue phase. The same scale factor is applied concurrently to both Drogues because each affects the simulated vehicle trajectory. The resulting scale factors for Drogues are generally close to unity because load measurements have already been adjusted based on IMU drag data. Therefore, the Drogue load test data are not scaled in the final step of peak load refinement. Sample FAST output loads are compared to flight data in Figure 14, where the peak loads again slightly overshoot the test data.

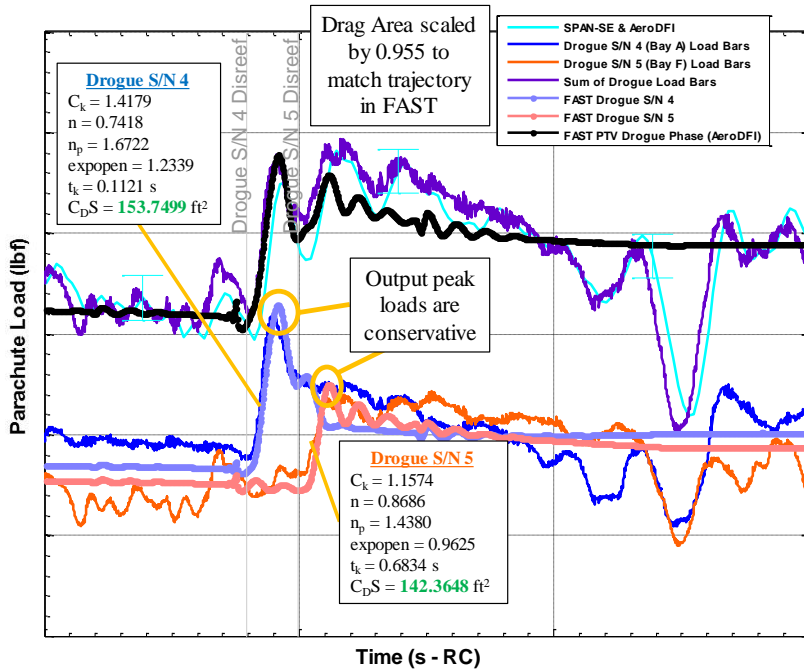


Figure 14. CQT-4-5 Drogue disreef to second stage FAST load output.

The peak load times and magnitudes for each stage are obtained from the test data by inspection and input as targets into the FAST python search routine. Each FAST run is conducted through the final disreef event because the optimization can be simultaneously performed on all stages to reduce computation time. Because only small adjustments are being made at each stage, a refinement of an early stage has little effect on later stages. Like with the FBCPs, each successive over-inflation factor is scaled by the ratio of target peak load to the current simulated peak load. Similarly, each successive value of peak fill constant is scaled by the ratio of the desired peak fill time to the current simulated peak fill time. The only

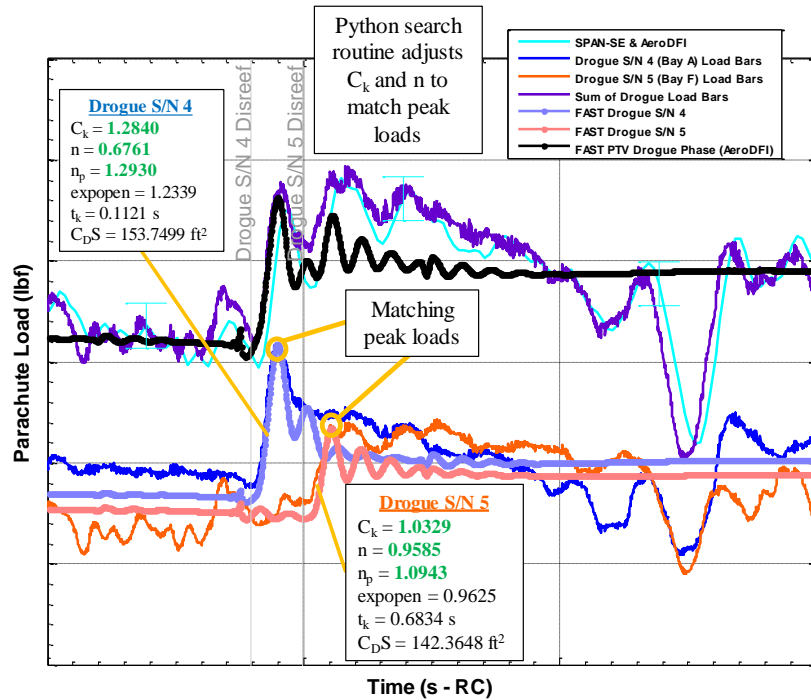


Figure 15. CQT-4-5 Drogue disreef to second stage FAST peak load matching.

difference for Drogues with respect to FBCPs is that the optimization is conducted for multiple stages at once. The resulting peak load match for this example is presented in Figure 15.

FAST Drogue reconstructions with this refinement method have generally reduced the magnitude of dispersed Drogue over-inflation factors and therefore reduced simulated Monte Carlo loads. For several tests, the optimum reconstructed over-inflation factor for disreefs was equal to 1.0, meaning that any over-inflation is due to added mass and spring force effects, not drag area growth.

C. Infinite Mass 3-D Monte Carlo Dispersion Limits

As tests with directly measured loads were initially performed on the FBCPs, a trend started to emerge with over-inflation factor. The FBCPs tended to have higher overall C_k values than Drogue first stage inflations, and the highest FBCP C_k values were higher than any Drogue experience, possibly due to the FBCP all-Kevlar construction. Because there is still not a statistically significant number of directly measured FBCP inflations, the FBCP distribution is a combination of directly-measured FBCP data and CPAS Drogue first stage inflation data (Section IV). Earlier analysis shifted the Drogue inflation data to match the median of the FBCP data. However, subsequent revised reconstructions of Drogue tests and additional FBCP data has brought the median of combined data set closer to the FBCP median, so the Drogue data are no longer shifted. The FBCP data are contained within the bounds of the composite distribution, which should be sufficient for prediction purposes. The median values for each data set are shown in the over-inflation histogram in the top of Figure 16. The FBCP peak fill constant and expopen distributions are each similar to those of first stage Drogues, with lognormal distributions. Therefore, the FBCP and Drogue data sets were combined into composite distributions, as shown on the center and bottom of the figure. Distributions are capped with bounds 10% beyond the lowest and highest test data.

Certain combinations of C_k , n_p , and expopen will result in excessively high or low loads outside of test experience. The reconstructed FBCP and Drogue first stage inflation parameters are plotted in three dimensions in the left of Figure 17. The upper and lower bounds of all three parameters provide eight combinations of drag area growth curves shown in the right of the figure. The combination of low n_p , low expopen, and high C_k will generate a load higher than any experienced in flight. Therefore, the test points can be bounded in all three dimensions using a convex hull algorithm (cyan). The engineering factor of 10% is then used to provide a buffer extending each outermost test point. The volume defined by this boundary (grey) is used to limit Monte Carlo draws. All three Monte Carlo parameters are drawn at the same time. Any 3-D point which lies outside the volume is rejected and re-drawn as necessary.

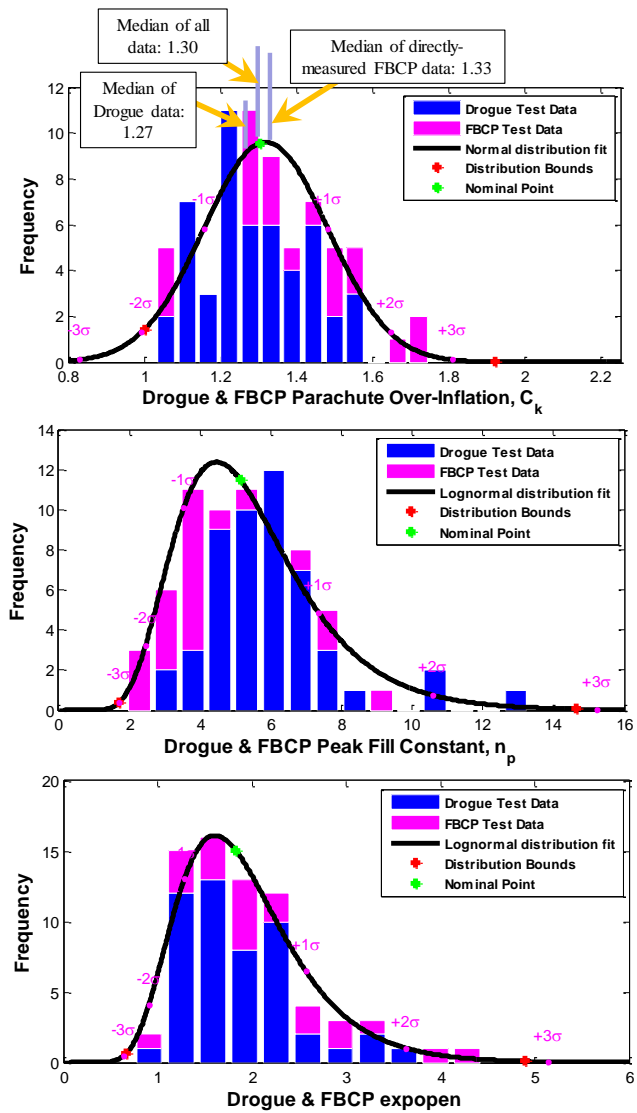


Figure 16. FBCP inflation parameters distributions compared with Drogue first stage parameters.

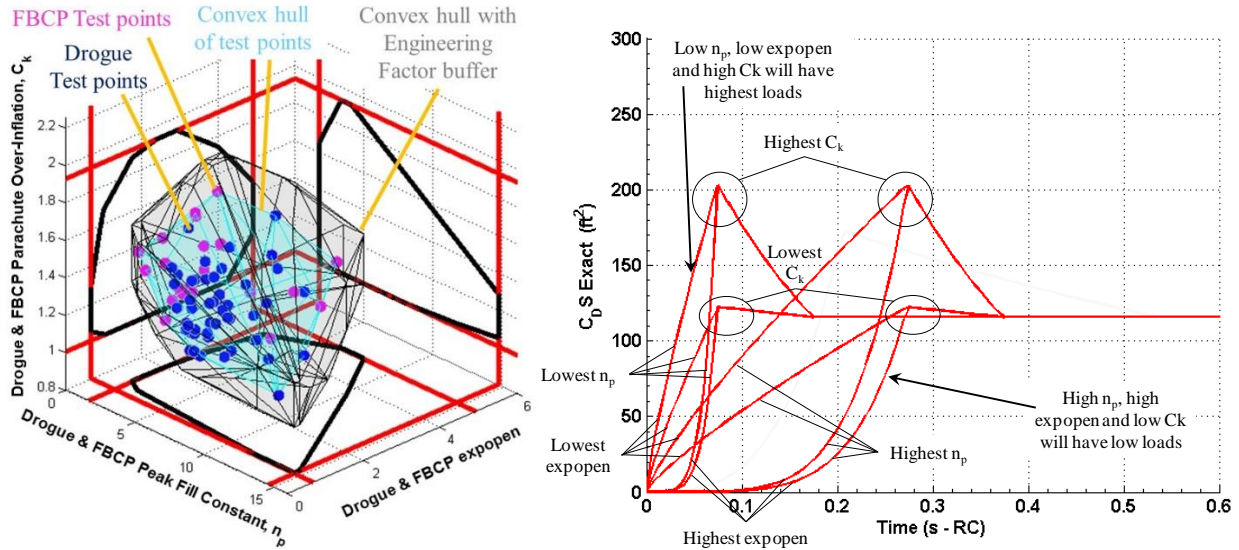


Figure 17. Reconstructed inflation parameters (left) and extreme drag area growth curves (right)

A sample of 10,000 Monte Carlo Drogue first stage inflation curves was generated to create the grey region in Figure 18. As expected, this region is bounded by the 10% engineering factor (black boundary) and encompasses reconstructed Drogue flight test data (blue). By design, the Monte Carlo region does not include the red curve corresponding to the highest theoretical load. Drogue disreef to second stage and full open parameters apply the same type of restrictions to ensure simulation output is physically possible.

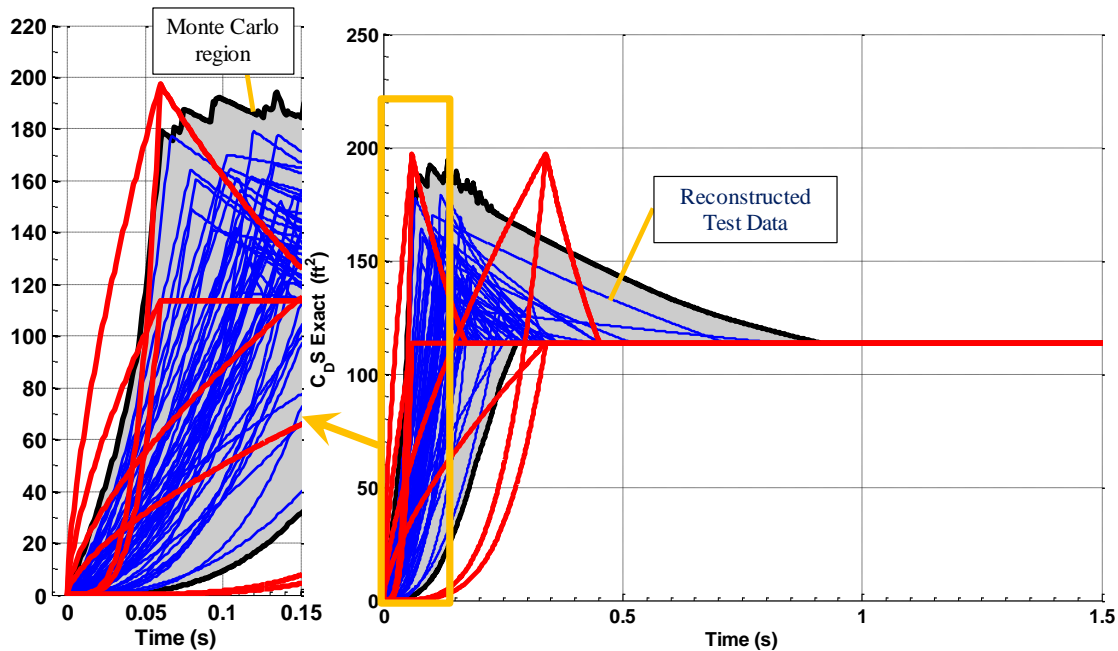


Figure 18. Drogue first stage drag area growth curves from flight test (blue) are bounded by the Monte Carlo region (grey), which does not include some extreme combinations (red)

V. Pilot Parachute Reconstruction

CPAS 9.85 ft D_o Conical Ribbon Pilot parachutes are deployed by mortars and lift the Main deployment bags in order to deploy the Main parachutes, as shown in Figure 19. Developing riser tension instrumentation for the Pilots was challenging, but data were eventually obtained which provided valuable insight into the Pilot performance. It was determined that Pilot inflation is finite mass under normal circumstances because the Pilots only lift a few hundred pounds and the loads do not act on the vehicle itself.

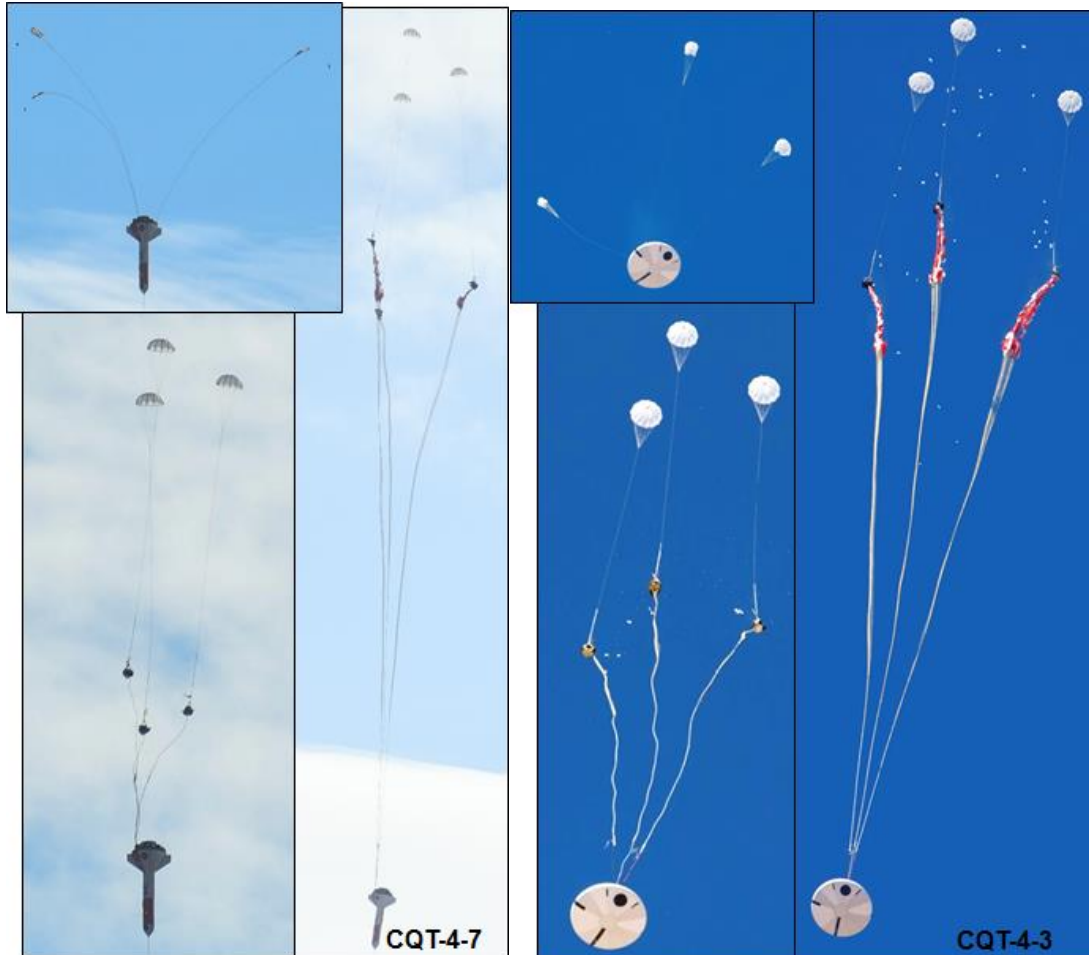


Figure 19. Pilot parachutes behind a PCDTV (left), and PTV (right).

Because the Pilot mortars have different orientations, each Pilot assembly follows a unique deployment trajectory prior to lifting its corresponding Main deployment bag, and the Mains will all reach bag strip at slightly different times. A method was developed to reconstruct Pilot inflation in FAST by matching event timing, even for tests where loads were not measured. This method was validated with the loads data which were available.

Due to some concern about the possible snatch force on the riser as the Main bag is lifted, a design change was made during the development phase to incorporate energy modulators into the Pilot risers. An Instrumented Main Bag Link (IMBL), similar to the production link, was installed between the Pilot parachute and Main bag to measure loads.

An example of IMBL data from CQT-4-3 is shown in Figure 20. Due to its location in the Pilot load train, the IMBL cannot be used to obtain data for use in the determination of Pilot inflation characteristics as the canopy would have already inflated before break ties (securing the IMBL) fail, the IMBL is lifted, and loads are recorded. As shown, the measured force reading is essentially zero during Pilot inflation. This prevents using inflation curve matching methods which are done with other parachutes. A large snatch force is measured when the Main bag retention system is overcome. Modeling such a force would require a significant modification to FAST. However, the peak simulated Pilot load is usually of a similar magnitude to the measured rebound force when the Main bag is lifted from the forward

bay. Because FAST does not include an energy modulator model, full loads reconstructions of the Pilots have not been possible since this design change went into effect.

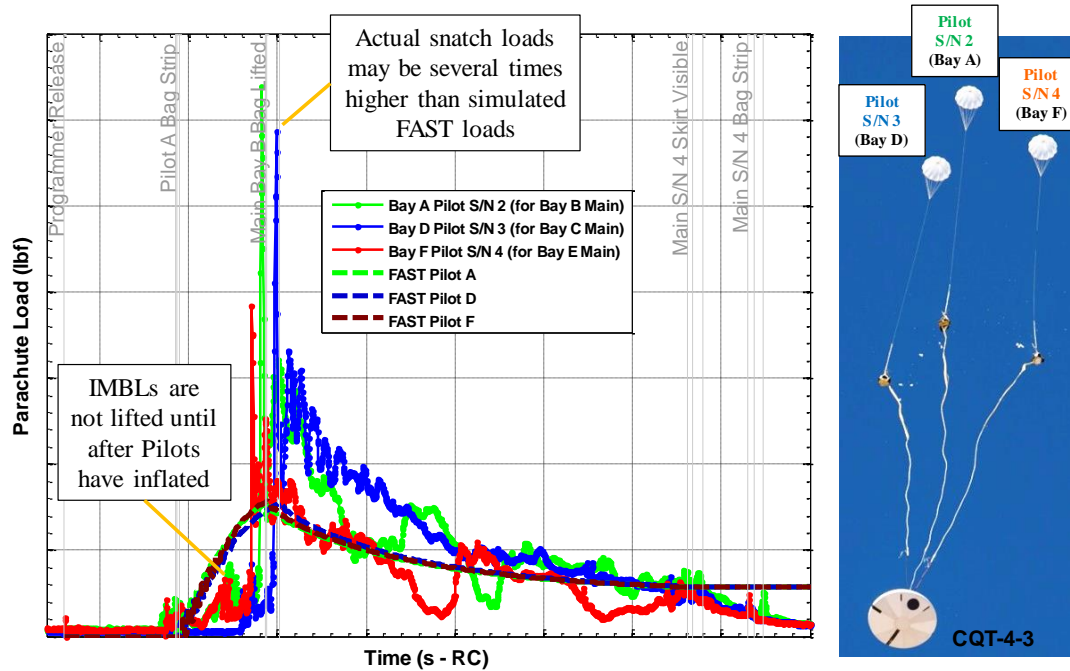


Figure 20. Sample Pilot load data compared to FAST reconstruction (without snatch load model).

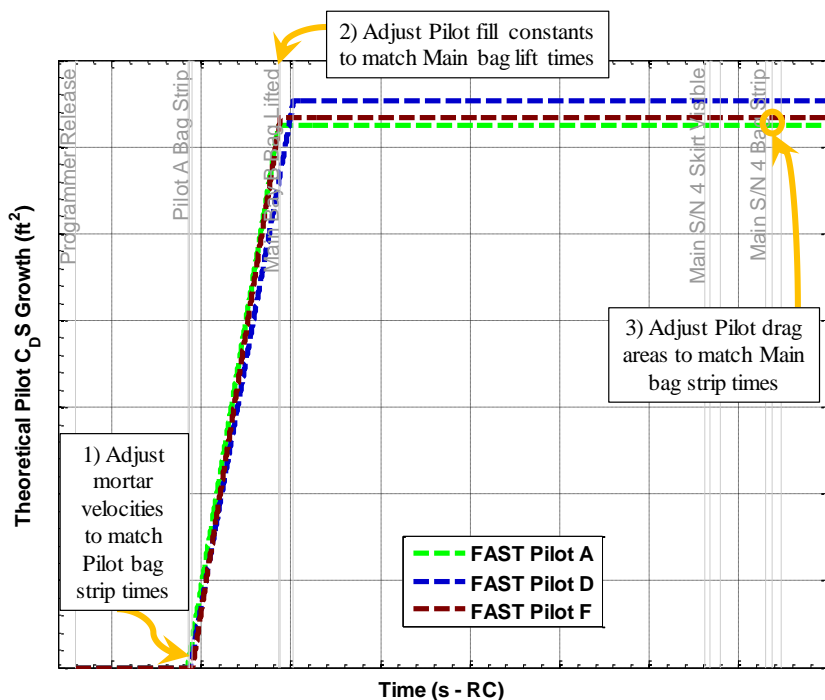


Figure 21. Pilot drag area timing reconstruction method.

Because of their function in deploying Main parachutes, the primary purpose of Pilot reconstructions is to support predicting Main deployment timing. The reconstruction method employs three FAST search routines to determine optimal inflation parameters to matching observed events from the video timeline. These are illustrated in the theoretical drag area growth curve of Figure 21. The first search adjusts Pilot mortar velocity until each simulated Pilot starts inflating at the actual time of Pilot bag strip. The second search adjusts each fill constant such that the fill time matches the actual time of the relevant Main bag lift. Due to the absence of inflation data, the drag growth shape is assumed to be linear by setting the expopen term to 1.0. Finally, each Pilot steady-

state drag area is adjusted such that the corresponding Main is deployed at the proper time.

Because the Pilot inflation is considered finite mass, reconstructed inflation parameters were collected to generate probability distributions in two dimensions (n and $expopen$), as shown in Figure 22. The majority of reconstructions use $expopen$ of 1.0. The exception is CDT-3-9 which employed the early design (without energy modulators) and

successfully matched inflation load shape data using a FAST-in-the-loop technique. The fill constant shows a clear central tendency and is fit to a lognormal distribution. The test data are bounded in both dimensions using the MATLAB convex hull algorithm (“convhull”) resulting in a test data polygon (cyan) bordering only the outermost points, as if it were a rubber band. A buffer (black polygon) around the test data polygon is then defined by extending the outermost test points by an engineering factor of 15%. The engineering factor for Pilots is larger than the customary value of 10% due to the relative lack of data and higher uncertainty. The upper- and lower-most bounds in both dimensions define the bounds on each distribution (red rectangle). In Monte Carlo simulations, random pairs of parameters are generated based on the probability distribution curves, and points within the black-bounded area only are retained as a means to avoid conditions outside of test experience. If the combination drawn is outside the buffer, both parameters are rejected and other pairs are drawn until the condition is satisfied. A set of 200,000 randomly dispersed Monte Carlo inputs were generated for each Pilot parachute in the cluster. The inset histogram shows the dispersed inputs for one of the Pilots.

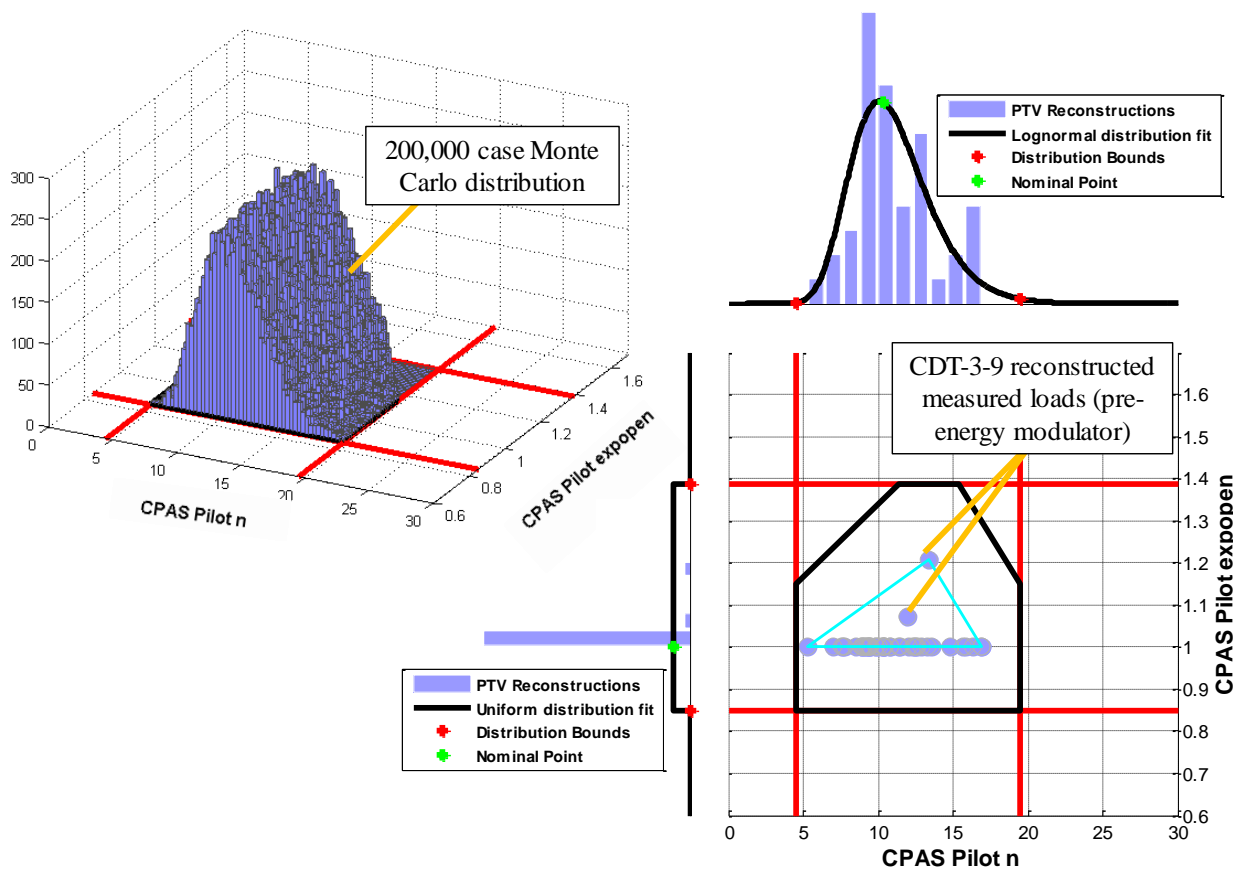


Figure 22. Pilot parachute finite mass inflation parameter probability distributions.

Pilot drag performance is strongly affected by the forebody wake. Reconstructions in a PTV wake had previously been performed while the CFD-derived Orion PRF model¹⁵ was active, while PCDTV reconstructions deactivate the model (see Section VII). However, it was known that the PRF model exaggerated the wake strength by assuming all parachutes are located in the strongest part of the wake, when in reality the Pilots are mortared perpendicular to the flow, and will therefore tend to spread out to areas of less extreme wake influence. In an update to the Pilot drag simulation method presented in Ref. 16, all Pilot reconstructions for Model Memo v18 now deactivate the model (set PRF to 1.0) so the quantity $PRF \cdot (C_D S)_p$ will be determined consistently for each relevant wake using statistical analysis. Early full open Drogue programmer data (with an older suspension line length ratio) are used as proxy sources of data to fill out the Pilot drag area distribution. Some freestream Pilot drag data were obtained at the HIVAS facility at China Lake, CA for reference.¹⁷ These other drag area sources were normalized to the Orion forebody using scaling.

VI. Main Parachute Reconstruction

Orion descends under a cluster of 116 ft D_o quarter spherical ringsail Main parachutes. CPAS is designed to make a safe landing under two of the nominal three canopies. The Mains undergo two reefed stages before inflating to full open, as shown in Figure 23. Test data have shown some variance in performance in first stage based on forebody shape, but the inclusion of PCDTV data will tend to make the resulting distribution more conservative for Orion predictions. It is assumed that forebody differences are negligible for second stage and full open.

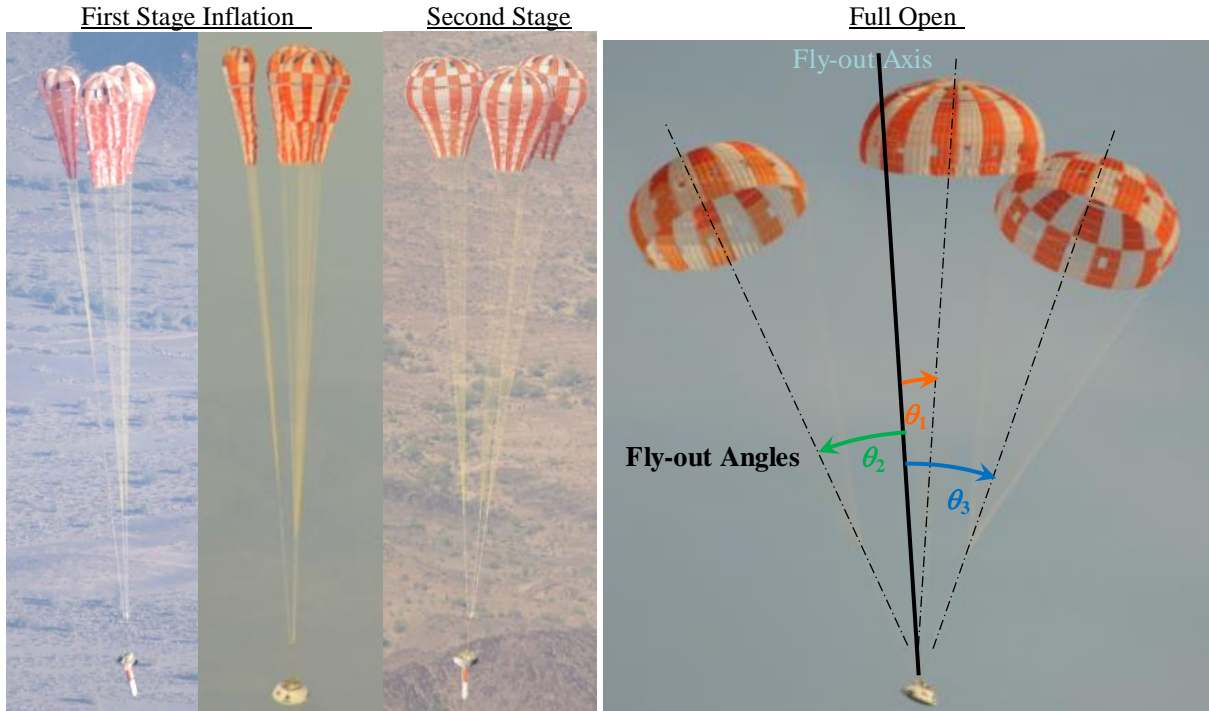


Figure 23. CPAS Main parachute stages.

The attachment mechanism for the Mains is very similar to the Drogues, so the method of compensating for lower load readings inside the vehicle structure is nearly the same. One difference is that the Mains have fairly large fly-out angles relative to a central axis.^{18,19} During steady-state, the IMU drag area is compared to the summation of the components of riser drag aligned with the deceleration vector by multiplying each individual canopy drag area by the cosine of its corresponding fly-out angle, θ , according to Eq. 7.

$$(C_D S)_p = \sum_{i=1}^{i=N_c} (C_D S)_{p,i} \cdot \cos \theta_i \quad (7)$$

A. Main Parachute First Stage Reconstruction

PTV test CQT-4-3 is taken as an example of the Main inflation reconstruction process. The first stage inflation drag area data are plotted in Figure 24. As with the Drogues, Main riser load measurements require scaling such that the time average of the sum of riser drag area matches the time average of cluster IMU drag area. Scale factors are specific to a given reefing stage and each is applied to all parachutes in the cluster. The MATLAB search routine is used to fit individual drag area data curves. The time average of the steady-state drag area for first or second stage depends on the endpoints chosen. However, sometimes those points are not evident, as a Main parachute stage often takes a long time to develop. Therefore, ending drag area was added as a search variable such that the output parachute parameters best fit the test data and are not dependent on the subjective choice of the engineer. For example, the MATLAB routine converged with Main S/N 4 growing to a full open drag area of 714 ft² about 6 seconds after bag strip. Had an earlier end time been chosen manually, the average drag area would be lower.

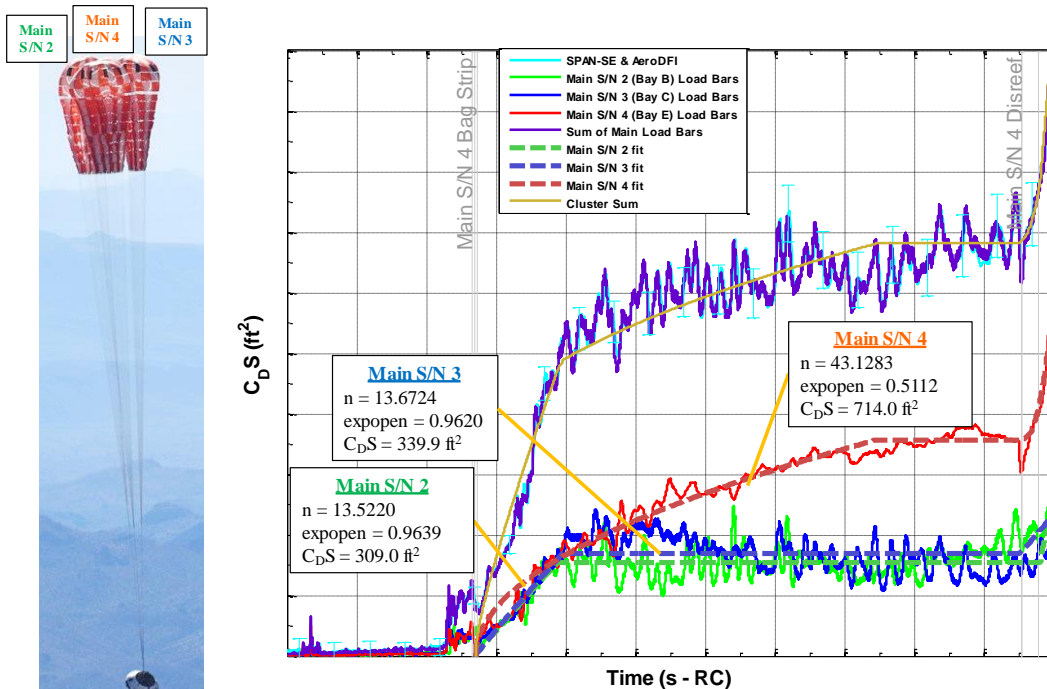


Figure 24. CQT-4-3 Main first stage drag area fit.

The FAST Main parachute simulation is initiated at Pilot mortar fire and is a continuation of the optimized Pilot parachute reconstruction in order to ensure each simulated Main deployment starts at the desired time. The MATLAB values of fill constant, exponential term, and drag area for each Main are transferred to the FAST input file. The only FAST search routine used is to match the altitude at disreef by varying a first stage steady-state drag scale factor. Like the Drogues, any adjustment is generally small because the load measurements were already scaled to match the total loads from the accelerometer.

The resulting peak loads from FAST are compared to measured peak loads in Figure 25. Instead of a constant inelastic load, the Mains employ a physics-based mass flow deployment model. The deployment model parameterizes the deploying Main parachute as a series of masses over discrete lengths. A table of cumulative mass is constructed from known physical properties of the Main parachute design. The deployment load is computed based on the change of momentum as components are re-accelerated to match the vehicle velocity. The load gradually builds up as the suspension lines deploy and load spikes are encountered as mass concentrations exit the deployment bag. FAST then begins the drag area growth model at simulated Main bag strip which determines individual inflation loads. In the example presented, both individual simulated loads

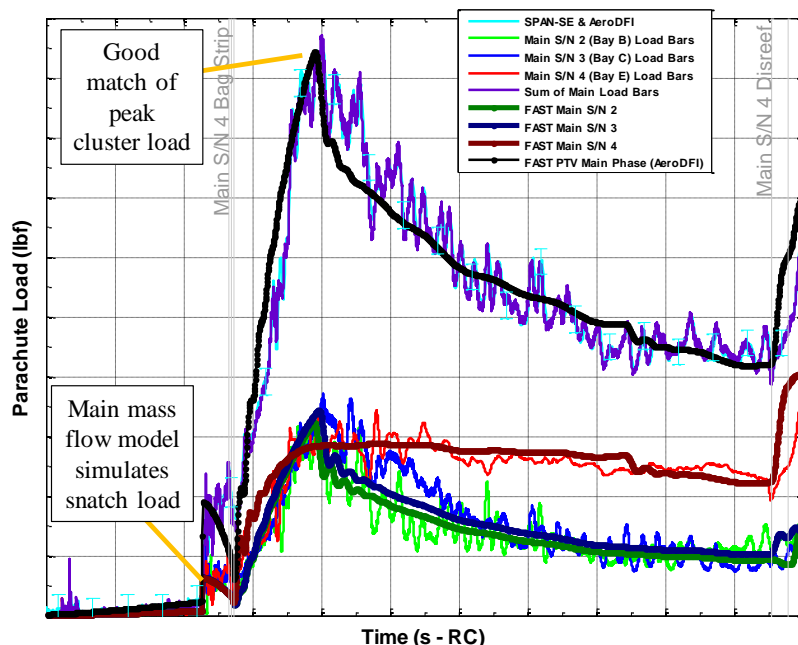


Figure 25. CQT-4-3 Main first stage FAST load output.

and the cluster peak load are in close agreement with the test data. Any large discrepancy must be accounted for by adjusting parameters manually, using engineering judgment because there are fewer input parameters to “tune” for finite mass inflation than for infinite mass inflation.

The reconstructed finite mass inflation parameters from relevant flight tests are collected together to generate probability distributions for each stage of Main inflation. The first stage histograms are plotted in 2-D in Figure 26 where both parameters are fit to lognormal distributions. The method for restricting dispersed Monte Carlo inputs is similar to that used by the Pilots, because both parachutes are modeled as finite mass. A combination of the lowest n and lowest expopen (lower left corner of the red box) will result in a sudden, concave up inflation C_D S trace. Because added mass is proportional to the rate of drag area growth, this condition will result in unrealistically high inflation loads. Conversely, a combination of the highest n and highest expopen (upper right corner) will result in unrealistically low loads due to slow drag area growth. Therefore, pairs of random draws are evaluated against the convex hull boundary with a 10% engineering factor (black) and re-drawn until they are within the prescribed region, therefore excluding the extreme possibilities outside flight experience. The inset histogram shows the probability distribution of a 200,000 case Monte Carlo input for a Main parachute.

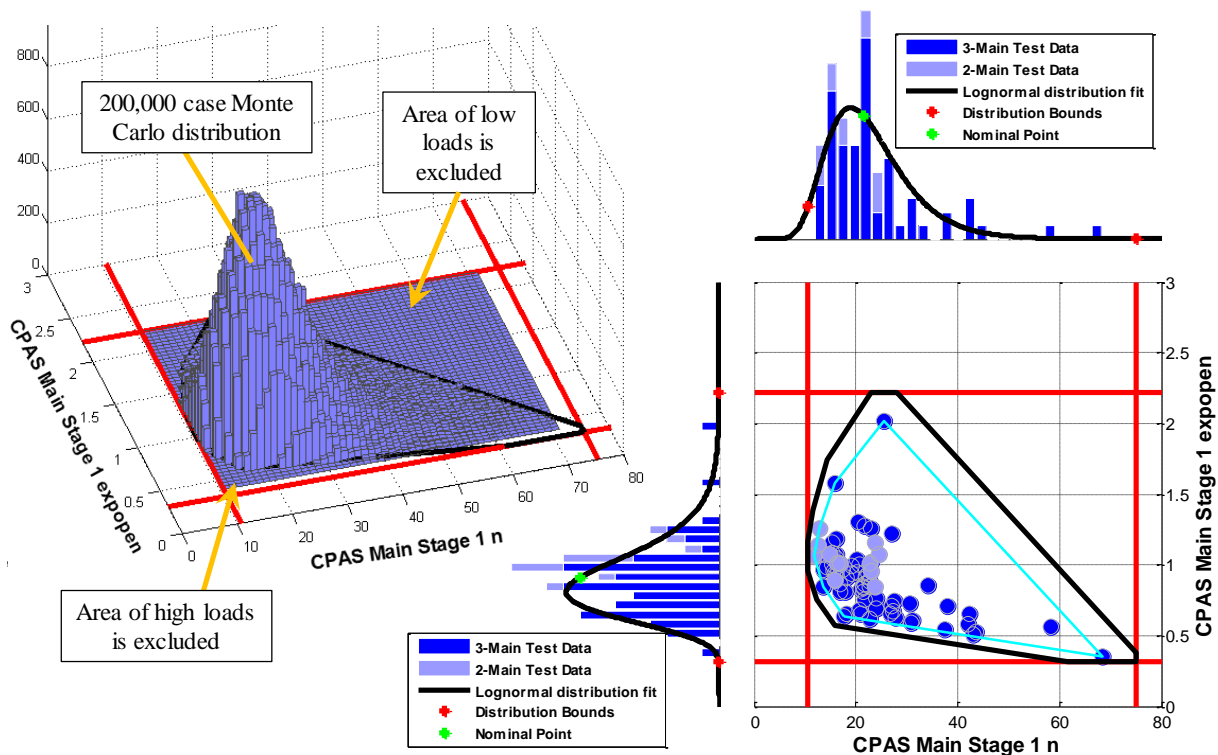


Figure 26. Main first stage finite mass inflation parameter probability distributions.

Sample drag area growth curves are plotted in red for all four extreme combinations of first stage n and expopen in Figure 27. The flight data (blue) are contained within the dispersion region (grey) which is bounded by the 10% engineering factor (black boundary). As expected, none of the dispersed cases have drag area growth similar to the extreme high and low load cases.

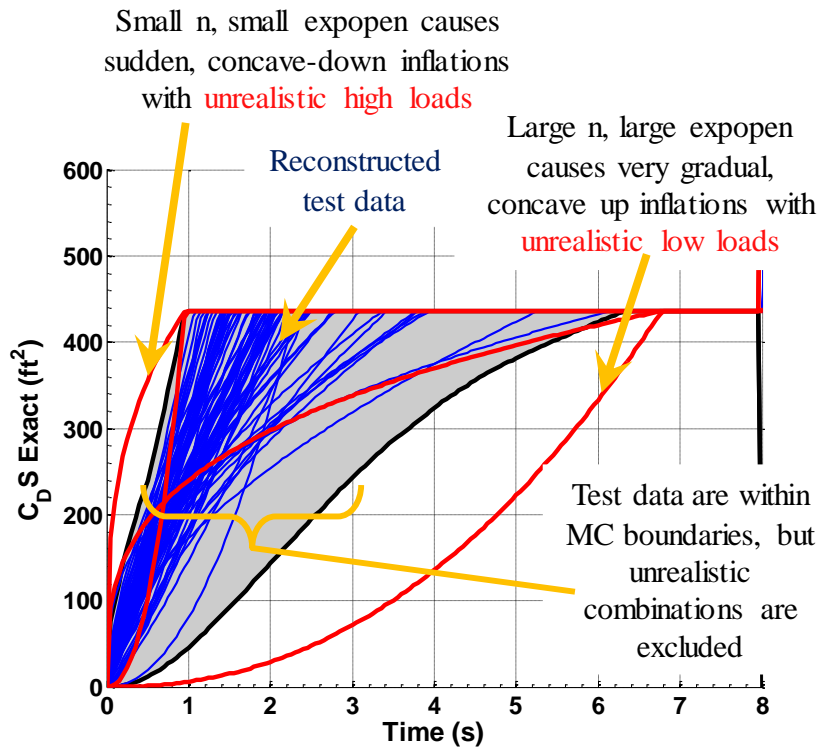


Figure 27. Sample Main drag area growth curves.

B. Main Parachute Disreef Reconstruction

The drag area data for Main second stage inflation is shown in Figure 28. The disreef timing for MATLAB and FAST is adjusted to match observations. MATLAB is used to determine fill constant, exponential term, and the steady-state drag area for each canopy in this stage. These values are then transferred to FAST.

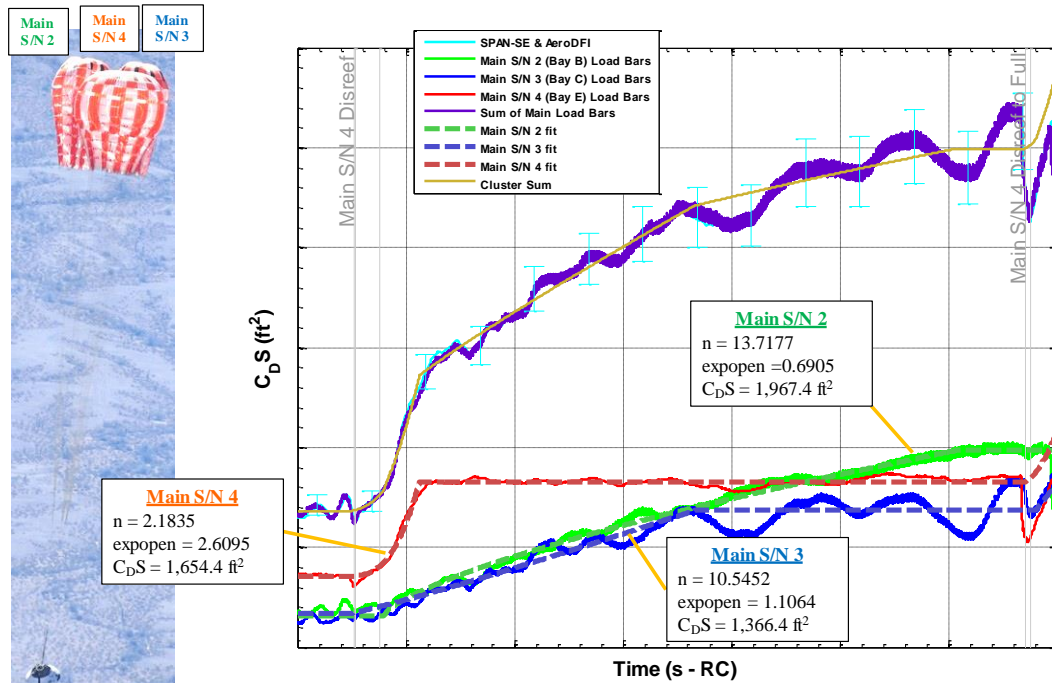


Figure 28. CQT-4-3 Main disreef to second stage drag area fit.

As with the first stage, a search is performed in FAST to determine the drag scale factor which results in matching the altitude at disreef to full open. The output loads from FAST (Figure 29) are generally close in magnitude to the test data, but inflation generally occurs more rapidly than in reality. In this case, the simulated peak load for the dominant canopy (S/N 4) exceeds the test data by about 19%.

The process for Main full open reconstruction is similar to second stage. Full open drag area data are plotted in Figure 30. The riser load readings for full open were scaled to match IMU drag area. As mentioned earlier, the total drag area for steady-state compensates for fly-out angles using Eq. 7. The fill constant and exponential terms are again determined by the MATLAB curve fit. By CPAS convention, final steady-

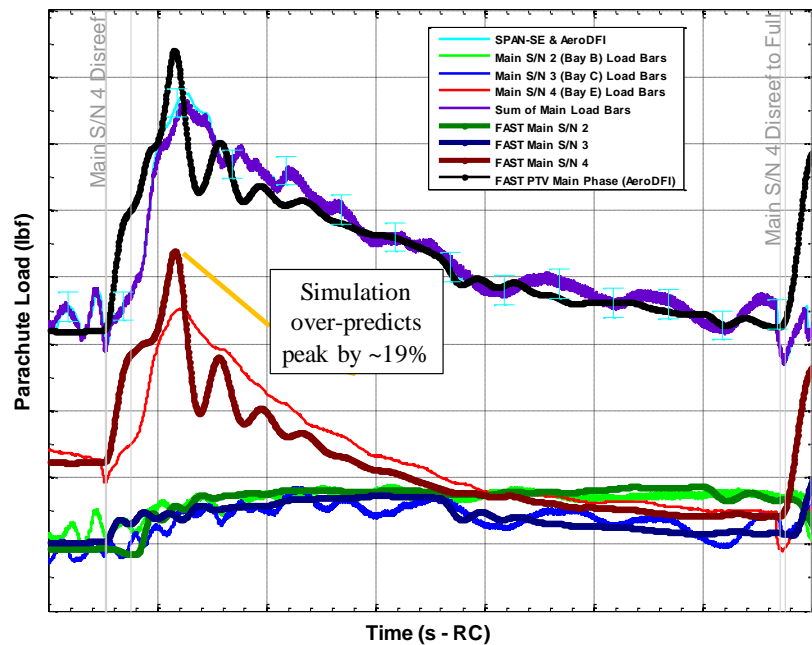


Figure 29. CQT-4-3 Main disreef to second stage FAST load output.

state drag area is derived from time averaged equilibrium rate of descent, $(C_D S)_o$,²⁰ rather than from load measurements, and all Mains are assumed to eventually level off to the same full open drag area value.

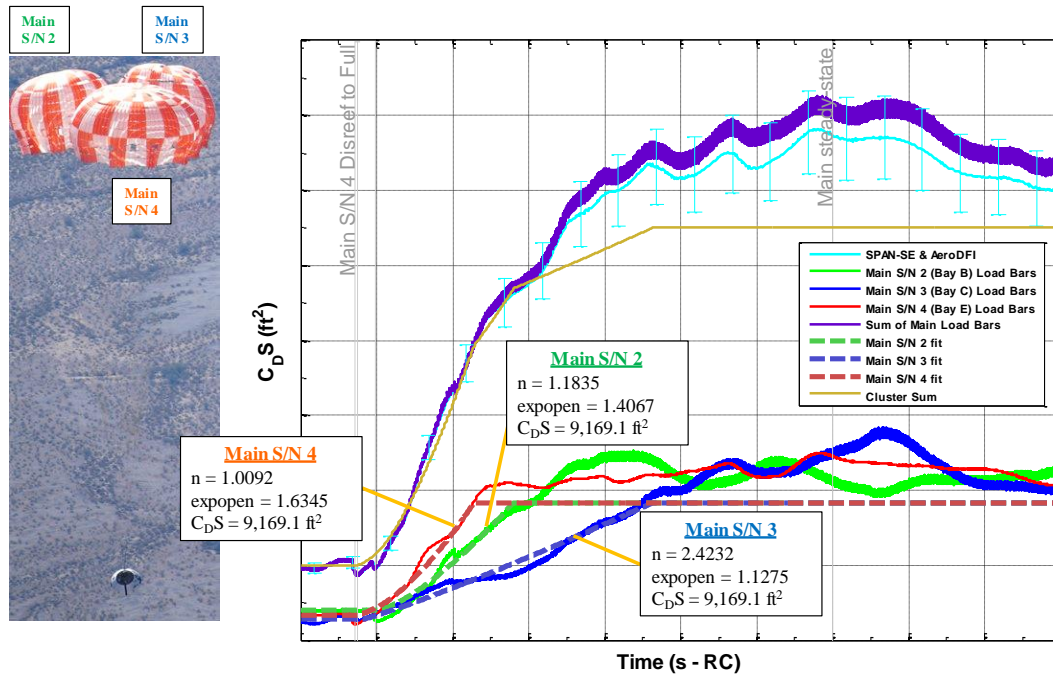


Figure 30. CQT-4-3 Main disreef to full open drag area fit.

Due to non-physical modeling of the added mass,²¹ the FAST peak disreef load usually occurs much earlier than the test data, as shown in Figure 31. However, the added mass model was calibrated such that the magnitude of simulated peak load is usually equal to or greater than the test data, so the model is conservative.

As discussed in Ref. 20, the statistical evaluation of rate of descent comes with its own challenges separate from those of parachute drag. This is because the Mains have significant cluster dynamics during steady-state that cause variations in vertical velocity. CPAS simulates the terminal phase of clusters of three Mains with an axisymmetric

time-varying rate of descent model which oscillates based on periodic data captured via photogrammetric analysis.²² Clusters of two Mains may have an additional complication with pendulum motion in the direction orthogonal to the parachute plane.²³ Therefore, a model was developed to independently simulate the aerodynamics of each parachute to evaluate landing under clusters of two Mains.²⁴

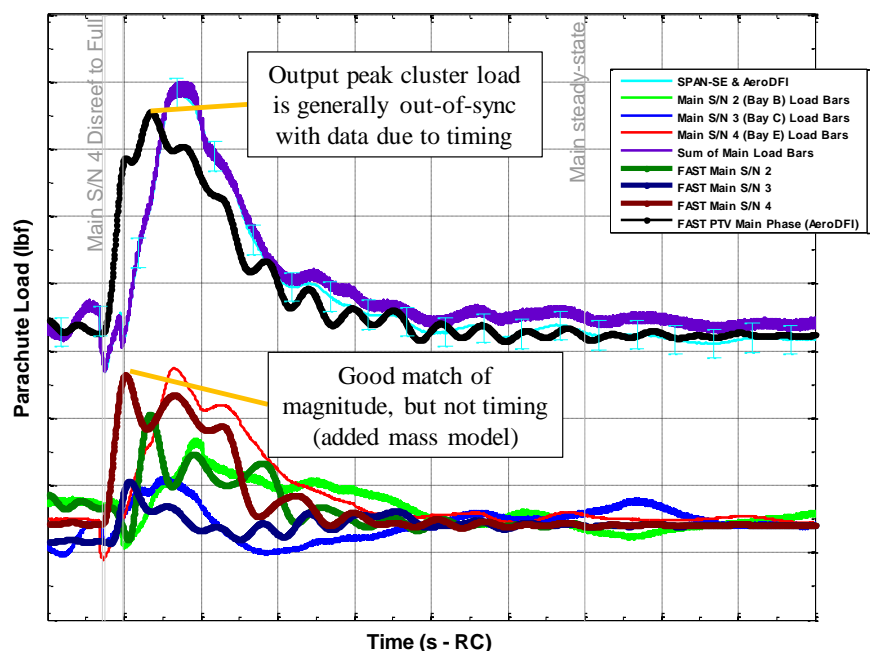


Figure 31. CQT-4-3 Main disreef to full open FAST load output.

VII. Forebody Wake and Other Effects on Drag Area

The methods for creating drag area distributions for CPAS parachutes, accounting for data collection behind various forebodies was previously described in Ref. 16. The completion of the CPAS test program provided an opportunity to update that analysis and evaluate certain assumptions of drag performance trends with the complete set of test data.

The first assumption under consideration is the estimation of parachute drag coefficient loss due to a wake in terms of trailing body diameters. The various parachute and forebody configurations which were evaluated are shown in the top of Figure 32. The plot is adapted from Fig. 5–21 of the Knacke design manual,²⁵ starting with legacy Apollo wake data, and augmented with Orion small scale Wind Tunnel Test (WTT) data^{26,27,28} and full scale CPAS tests.

Drag coefficient loss is equivalent to PRF, which requires parachute performance data in a clean wake. Starting with the closest to freestream conditions (right-most on the plot), the Pilot parachutes were tested with no forebody at HIVAS.¹⁷ Initial testing of the FBCPs was done with extremely small payloads, approximating a clean wake. Single Drogues were used as programmers and test articles during early Drogue Development Tests (DDT) and Main Development Tests (MDT). Due to its small diameter (24 inches) and slender shape, the Medium Drop Test Vehicle (MDTV) was assumed to only generate a negligible wake during these tests. However, those tests used the original Drogue suspension line length ratio ($L_s/D_o = 1.5$) and no full open Drogue data is available with a clean wake for the current length ($L_s/D_o = 2.0$). Therefore, Drogue PRF estimations are limited to reefed configurations, for which the line length ratio is not a factor.

The PCDTV was also streamlined, but flared out to 106 inches at the aft end to accommodate the parachute compartment and was expected to generate a measurable wake. The PTV has a diameter 198 inches, to simulate the full scale Orion heatshield, and therefore generates the strongest wake. CPAS flight data has generally matched the expectation that wake degradation is strongest for parachutes with smaller projected diameters (D_p) behind vehicles with the largest forebody diameter (D_B) with the shortest trailing distances (L_T). There is considerable test-to-test scatter in the data, where individual data points often show a PRF greater than unity. However, the average PRF performance for a given configuration (indicated by horizontal dashed lines) are all less than 1.0 and usually terminate within the envelope of legacy data. A notable exception is performance of Pilot parachutes, especially in a PCDTV wake, which have lower drag than expected. This may be due to the fact that drag is not measured directly on Pilot reconstructions, but is inferred through the timing of Main parachute deployment in FAST. Early Pilot Development Tests (PDT) did measure Pilot drag, but were conducted with an older ringslot canopy design and are therefore not relevant to the current conical ribbon design.

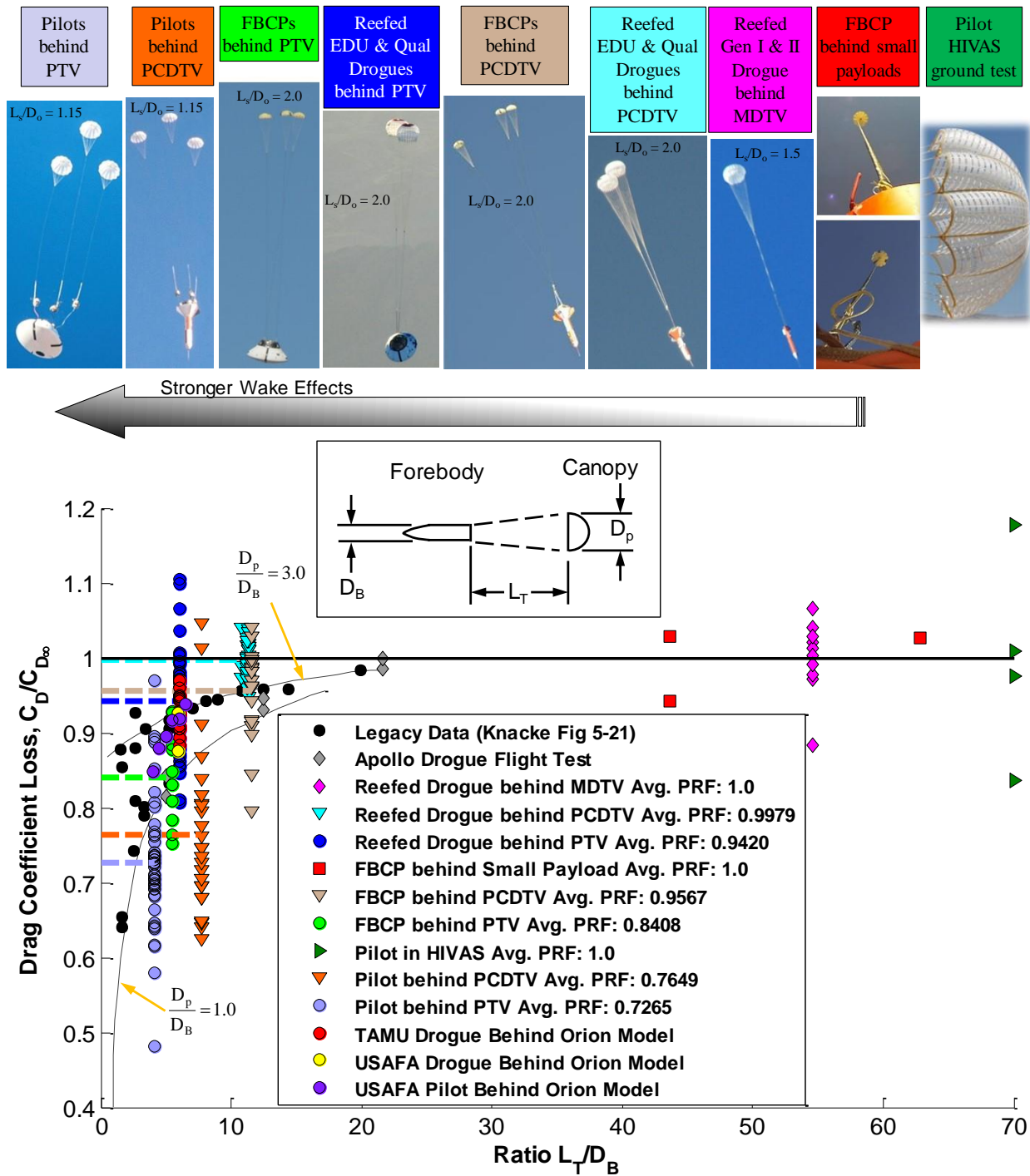


Figure 32. CPAS canopy drag loss caused by forebody wake compared to legacy and wind tunnel data.

PRF computations are summarized in Table 1. The PRF behind the MDTV is assumed to be 1.0 and the Main parachute is assumed to have negligible forebody effects (evaluated below). Reefed Drogues seem to have very similar performance behind a PCDTV as an MDTV (with a PRF slightly greater than 1.0 for first stage). However, because the reefing lengths for Drogues have changed over the course of the test program, PRF was inferred via trend-lines and which may mask some PCDTV wake effects. Although there is no full open Drogue drag data from which to compute PRF, it can be useful to compute the relative performance between PTV and PCDTV forebodies, as listed in the right-most column.

Table 1. Summary of CPAS PRF Behind Test Forebodies

Parachute	Average Pressure Recovery Fraction			Ratio of Forebody Performance (C_{dS}) _{PTV} / (C_{dS}) _{PCDTV}
	Behind MDTV/Clean	Behind PCDTV	Behind PTV/Orion	
FBCP	1.0 (assumed)	0.9567	0.8408	0.8788
Drogue first stage	1.0 (assumed)	1.0004	0.9372	0.9369
Drogue second stage	1.0 (assumed)	0.9935	0.9465	0.9527
Drogue full open	No clean wake data for normalization			0.9681
Pilot	1.0 (assumed)	0.7649	0.7265	0.9499
Main	1.0 (assumed)	~1.0 (assumed)	~1.0 (assumed)	~1.0 (assumed)

Some assumptions of the influences of full open Drogue performance are investigated in Figure 33. Individual drag area test points are plotted for various configurations of line length ratio, number of parachutes, and forebody type. The average values for each configuration are plotted as short horizontal lines. Only certain combinations of factors were tested with varying sample sized. In addition to flight test data, a 10% scale fabric Drogue was tested at the Texas A&M (TAMU) Oran W. Nicks subsonic wind tunnel (10'x7') with both line length ratios. The absolute drag of the TAMU data does not appear to be accurate due to scaling and blockage effects, but it does provide sensitivity effects for different configurations.

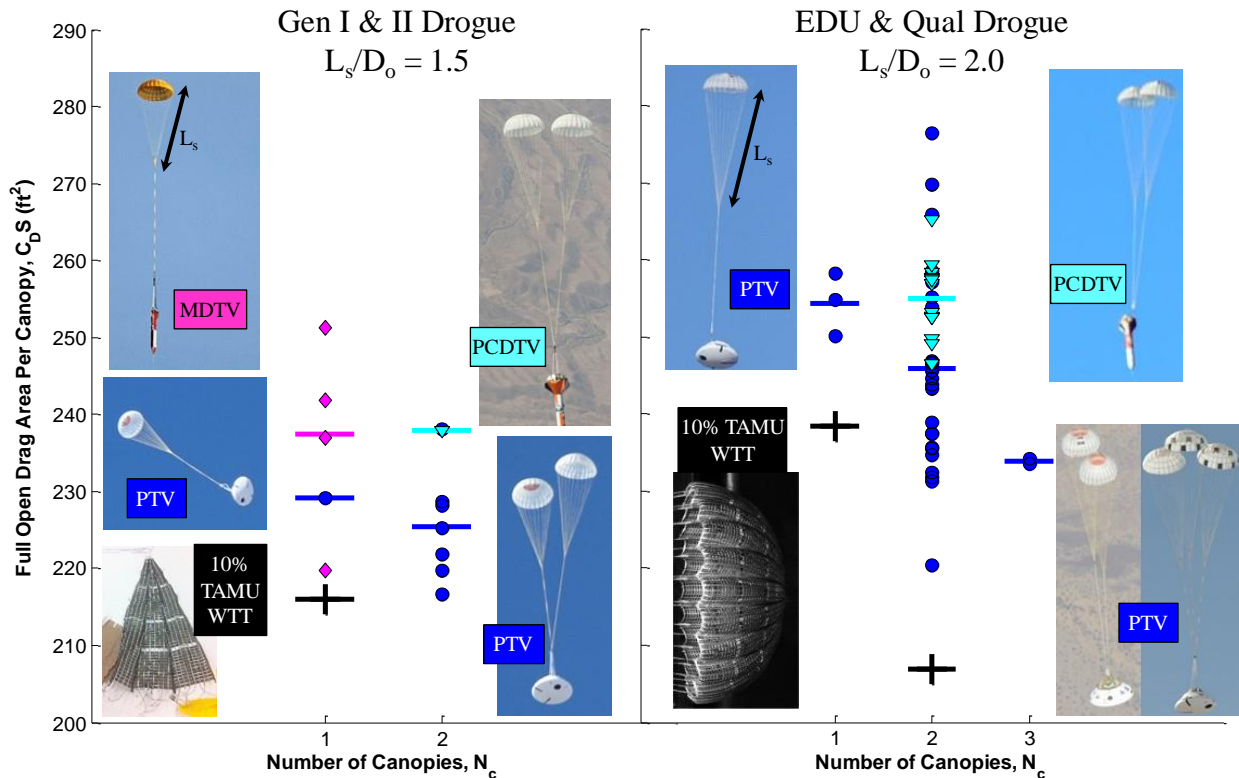


Figure 33. Full open Drogue performance comparison for design (L_s/D_o), number of canopies, and forebody type.

As expected, the increase in line length ratio from 1.5 (left) to 2.0 (right) resulted higher drag when other factors were held constant. The amount of drag increase was about 10% for a single Drogue configuration and about 7% to 9% for the dual Drogue configuration, as summarized in Table 2.

Table 2. Drogue Full Open Drag Area Performance Improvement with L_s/D_0 from 1.5 to 2.0

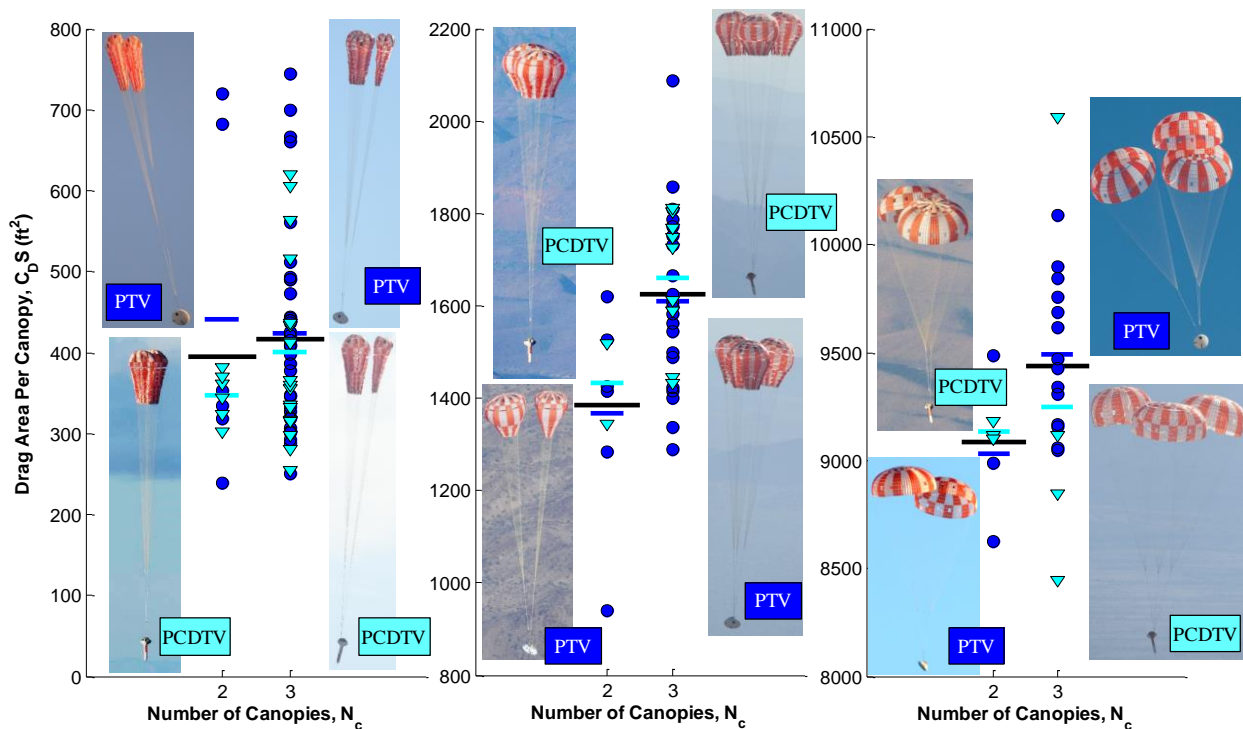
Forebody	1 Drogue	2 Drogue
10% TAMU WTT (no wake)	1.1038	N/A
PCDTV	N/A	1.0716
PTV	1.1105	1.0905

Early in the CPAS program, a decision was made to assume that the performance of a single Drogue parachute was the same as for a cluster of two in order to maximize the statistical significance of the limited available test data. According to Table 3, the actual decrease in performance in flight behind a PTV was less than what was predicted via wind tunnel. Actual performance loss is only about 1.5% to 3.3%, reinforcing the decision to group single and dual Drogue flight test data. The performance drop with a cluster of three Drogue parachutes approaches 10%, and should therefore be accounted for in flight test planning (predicted distributions for a cluster of three Drogues are published in the CPAS Test Technique Memo).

Table 3. Drogue Full Open Drag Area Performance Decrease with Number of Parachutes

Forebody	$L_s/D_0 = 1.5$	$L_s/D_0 = 2.0$	
	N_{c2} / N_{c1}	N_{c2} / N_{c1}	N_{c3} / N_{c1}
10% TAMU WTT (no wake)	N/A	0.8676	N/A
PCDTV	N/A	N/A	N/A
PTV	0.9843	0.9666	0.9194

A similar analysis was performed for all stages of Main parachutes in Figure 34. Performance differences due to the number of canopies in the cluster and the type of forebody were evaluated. It had always been assumed that forebody effects are minor for such large parachutes. Such effects, if any, should be most significant during the first reefed stage. However, the average performance behind a PTV is actually higher than that for a PCDTV for first stage and trades off for later stages. This implies that the forebody effect is simply random and that data can be grouped irrespective of test vehicle.

**Figure 34. Main performance comparison for number of canopies and forebody type for first stage (left), second stage (center), and full open (right).**

The average values for composite Main parachute data sets are plotted as longer horizontal black lines. These indicate a consistent increase in Main parachute efficiency when the cluster size increases from two to three. This effect has been observed in reefed stages since early in the test program and is due to parachute interference effects. The canopies in a cluster of two will tend to come in close proximity and elongate the reefed opening, resulting in less available inlet area than for clusters of three, which tend to spread further apart with less elliptical openings. For full open, the two Main configuration has limited ability to damp motion induced by air flows perpendicular to the parachute plane, which can result in significant gliding and perhaps even large pendulum motion, as described in Ref. 23. The three Main configuration has less oscillation, and therefore higher overall average performance.

VIII. Conclusion

As Orion approaches certification for human flight, the methods for predicting CPAS performance based on flight test reconstructions have undergone refinement. Multiple high quality sensors contribute to a reduction in data uncertainty. Automated search routines in the FAST simulation improve the accuracy of reconstructions and removes subjectivity from the process.

Like data are collected whenever possible to maximize statistical significance of parameter distributions. These parameters are used to generate Monte Carlo dispersed inputs, which are restricted such that extreme combinations do not stray far outside test experience. Many of the assumptions for grouping data were confirmed using the full test database. Simulations of the final design can therefore be used confidently to qualify the system for safely landing personnel.

Acknowledgments

The author wishes to thank Phil Stuart and other members of the NASA Orion MPCV Aeroscience Team for providing PTV forebody drag data which has greatly improved the quality of parachute results.

Trade names and trademarks are used in this report for identification only. Their usage does not constitute an official endorsement, either expressed or implied, by the National Aeronautics and Space Administration.

References

- ¹Ray, E. S., and Morris, A. L., "Challenges of CPAS Flight Testing," *21st AIAA Aerodynamics Decelerator Systems Technology Conference*, Dublin, Ireland, May 2011, AIAA paper 2011-2557.
- ²Moore, J. W., and Morris, A. L., "Development of Monte Carlo Capability for Orion Parachute Simulations," *21st AIAA Aerodynamics Decelerator Systems Technology Conference*, Dublin, Ireland, May 2011, AIAA paper 2011-2610.
- ³Moore, J. W. and Romero, L. M., "A Boilerplate Capsule Test Technique for the Orion Parachute Test Program," *22nd AIAA Aerodynamic Decelerator Systems Technology Conference*, Daytona Beach, Florida, March 2013, AIAA paper 2013-1290.
- ⁴Moore, J. W. and Romero, L. M., "An Airborne Parachute Compartment Test Bed for the Orion Parachute Test Program," *22nd AIAA Aerodynamic Decelerator Systems Technology Conference*, Daytona Beach, Florida, March 2013, AIAA paper 2013-1289.
- ⁵NovAtel, Inc., "IMU-HG," NovAtel, Inc. web site [online], 2009, URL: http://www.novatel.com/assets/Documents/Papers/HG1700_SPAN58.pdf [cited 18 August 2010].
- ⁶NovAtel, Inc., "SPAN-SE," NovAtel, Inc. web site [online], February 2010, URL: <http://novatel.com/Documents/Papers/SPAN-SE.pdf> [cited 23 March 2010].
- ⁷Cuthbert, P., "Decelerator System Simulation (DSS) Version 312," June 2010, NASA, Houston, TX.
- ⁸Ray, E., "Reconstruction of Orion EDU Parachute Inflation Loads," *22nd AIAA Aerodynamic Decelerator Systems Technology Conference*, Daytona Beach, Florida, March 2013, AIAA paper 2013-1260.
- ⁹Ray, E., "CPAS Operating Modeling Parameters Version 18 (System Acceptance Review)," NASA JSC 65914 Rev. M, June 2019.
- ¹⁰Ray, E., "CPAS Simulation of Drop Test Vehicles and Test Techniques Version 18," JETS-JE11-13-SAIP-MEMO-0021 Rev. H, JSC Engineering Technology and Science contract, Jacobs Engineering, June 2019.
- ¹¹Romero, L. and Ray, E., "Application of Statistically Derived CPAS Parachute Parameters," *22nd AIAA Aerodynamic Decelerator Systems Technology Conference*, Daytona Beach, Florida, March 2013, AIAA paper 2013-1266.
- ¹²Fraire, U., Dearman, J., and Morris, A. L., "Proposed Framework for Determining Added Mass of Orion Drogue Parachutes," *21st AIAA Aerodynamics Decelerator Systems Technology Conference*, Dublin, Ireland, May 2011, AIAA paper 2011-2546.
- ¹³Cassady, L. D., Ray, E. S., and Truong, T. H., "Aerodynamic Reconstruction Applied to Parachute Test Vehicle Flight Data Analysis," *22nd AIAA Aerodynamic Decelerator Systems Technology Conference*, Daytona Beach, Florida, March 2013, AIAA paper 2013-1259.
- ¹⁴Schulte, P. Z., Moore, J. W., and Morris, A. L., "Verification and Validation of Requirements on the CEV Parachute Assembly System Using Design of Experiments," *21st AIAA Aerodynamics Decelerator Systems Technology Conference*, Dublin, Ireland, May 2011, AIAA paper 2011-2558.
- ¹⁵Stuart, Phil C., "Orion Crew Module Pressure Recovery Fractions", EG-CAP-12-27, 22 March 2012, NASA/JSC EG3.
- ¹⁶Ray, E., "Test Vehicle Forebody Wake Effects on CPAS Parachutes," *24th AIAA Aerodynamic Decelerator Systems Technology Conference*, Denver, Colorado, June 2017, AIAA paper 2017-3227.
- ¹⁷Ray, E. S., Hennings, E., and Bernatovich, M. A., "Testing Small CPAS Parachutes Using HIVAS," *22nd AIAA Aerodynamic Decelerator Systems Technology Conference*, Daytona Beach, Florida, March 2013, AIAA paper 2013-1309.
- ¹⁸Ray, E. S., Bretz, D. R., and Morris, A. L., "Photogrammetric Analysis of CPAS Main Parachutes," *21st AIAA Aerodynamics Decelerator Systems Technology Conference*, Dublin, Ireland, May 2011, AIAA paper 2011-2538.
- ¹⁹Ray, E. S. and Bretz, D. R., "Improved CPAS Photogrammetric Capabilities for Engineering Development Unit (EDU) Testing," *22nd AIAA Aerodynamic Decelerator Systems Technology Conference*, Daytona Beach, Florida, March 201, AIAA paper 2013-1258.
- ²⁰Ray, E. S., and Morris, A. L., "Measurement of CPAS Main Parachute Rate of Descent," *21st AIAA Aerodynamics Decelerator Systems Technology Conference*, Dublin, Ireland, May 2011, AIAA paper 2011-2545.
- ²¹Ray, E., "Isolating Added Mass Load Components of CPAS Main Clusters," *24th AIAA Aerodynamic Decelerator Systems Technology Conference and Seminar*, Denver, Colorado, June 2017, AIAA paper 2017-3232.
- ²²Ray, E., "A Symmetric Time-Varying Cluster Rate of Descent Model," *23rd AIAA Aerodynamic Decelerator Systems Technology Conference*, Daytona Beach, Florida, March 2015, AIAA paper 2015-2137.
- ²³Ray, E. and Machin, R. A., "Pendulum Motion in Main Parachute Clusters," *23rd AIAA Aerodynamic Decelerator Systems Technology Conference*, Daytona Beach, Florida, March 2015, AIAA paper 2015-2138.
- ²⁴Ali, Y., Sommer, B., *et al.*, "Orion Multi-Purpose Crew Vehicle Solving and Mitigating the Two Main Cluster Pendulum Problem," *24th AIAA Aerodynamic Decelerator Systems Technology Conference*, Denver, Colorado, June 2017, AIAA paper 2017-4056.
- ²⁵Knacke, T. W., "Parachute Recovery Systems Design Manual", Para Publishing, Santa Barbara, California, 1992.
- ²⁶Sengupta, A., *et al.*, "Performance of a Subscale CPAS Conical Ribbon Drogue Parachute in a Turbulent Wake," *22nd AIAA Aerodynamic Decelerator Systems Technology Conference*, Daytona Beach, Florida, March 2013, AIAA paper 2013-1307.
- ²⁷Becker, J., Johnson, S., and Yechout, T., "Investigation of NASA Orion Wake Effects on Drogue Chute Aerodynamic Characteristics," *21st AIAA Aerodynamic Decelerator Systems Technology Conference and Seminar*, Dublin, Ireland, May 2011, AIAA paper 2011-2539.
- ²⁸Kolesar, R. and Yechout, T., "Experimental Investigation of NASA Orion Pilot Chute Drag Characteristics," *22nd AIAA Aerodynamic Decelerator Systems Technology Conference*, Daytona Beach, Florida, March 2013, AIAA paper 2013-1355.